

UNCLASSIFIED

SECURITY CLASSIFICATION OF THIS PAGE

ADA201380

REPORT DOCUMENTATION PAGE				Form Approved OMB No. 0704-0188	
1a REPORT SECURITY CLASSIFICATION UNCLASSIFIED		1b RESTRICTIVE MARKINGS			
2a SECURITY CLASSIFICATION AUTHORITY		3 DISTRIBUTION / AVAILABILITY OF REPORT Approved for public release; distribution is unlimited.			
2b DECLASSIFICATION / DOWNGRADING SCHEDULE					
4 PERFORMING ORGANIZATION REPORT NUMBER(S) ARL-TR-88-17		5 MONITORING ORGANIZATION REPORT NUMBER(S)			
6a NAME OF PERFORMING ORGANIZATION Applied Research Laboratories		6b OFFICE SYMBOL (if applicable) ARL:UT		7a NAME OF MONITORING ORGANIZATION	
6c ADDRESS (City, State, and ZIP Code) The University of Texas at Austin P.O. Box 2029 Austin, Texas 78713-8029		7b ADDRESS (City, State, and ZIP Code)			
8a NAME OF FUNDING / SPONSORING ORGANIZATION Office of Naval Research		8b OFFICE SYMBOL (if applicable) ONR		9 PROCUREMENT INSTRUMENT IDENTIFICATION NUMBER N00014-87-K-0346	
8c ADDRESS (City, State, and ZIP Code) Department of the Navy Arlington, Virginia 22217-5000		10 SOURCE OF FUNDING NUMBERS			
		PROGRAM ELEMENT NO	PROJECT NO	TASK NO	WORK UNIT ACCESSION NO
11 TITLE (Include Security Classification) A Frequency Dependent Ray Theory					
12 PERSONAL AUTHOR(S) Foreman, Terry L.					
13a TYPE OF REPORT technical		13b TIME COVERED FROM _____ TO _____		14 DATE OF REPORT (Year, Month, Day) 88-3-28	
15 PAGE COUNT 76					
16 SUPPLEMENTARY NOTATION					
17 COSATI CODES			18 SUBJECT TERMS (Continue on reverse if necessary and identify by block number)		
FIELD	GROUP	SUB-GROUP	→ ray theory; acoustic propagation. <i>1/12/88</i>		
19 ABSTRACT (Continue on reverse if necessary and identify by block number)					
<p>Practical computational procedures for obtaining ray theoretical solutions to the inhomogeneous Helmholtz equation resort to a well known approximation. The computational method presented here enables one to trace rays without resort to the ray theory approximation provided a solution to the Helmholtz equation is available by independent means. In other words, given a solution to the Helmholtz equation, the exact rays for that case can be computed. The new ray theory therefore serves, not as a computational method, but as a new method of displaying solutions to the Helmholtz equation.</p> <p><i>Key: 1/12/88</i></p>					
20 DISTRIBUTION / AVAILABILITY OF ABSTRACT <input type="checkbox"/> UNCLASSIFIED/UNLIMITED <input checked="" type="checkbox"/> SAME AS RPT <input type="checkbox"/> DTIC USERS			21 ABSTRACT SECURITY CLASSIFICATION UNCLASSIFIED		
22a NAME OF RESPONSIBLE INDIVIDUAL Thomas A. Griffy			22b TELEPHONE (Include Area Code) 512-835-3489		22c OFFICE SYMBOL DO

UNCLASSIFIED

TABLE OF CONTENTS

	<u>Page</u>
LIST OF FIGURES	v
PREFACE	vii
I INTRODUCTION	1
II OCEANIC ACOUSTIC WAVE PROPAGATION	3
A. THE LAGRANGIAN DENSITY	3
B. THE ACOUSTIC WAVE EQUATION	5
C. THE HELMHOLTZ EQUATION	6
1. Sources and boundary conditions	7
2. Attenuation	8
III REVIEW OF RAY THEORY	11
A. THE RAY PATH AND TRANSPORT EQUATIONS	11
B. CONSERVATION OF ENERGY	13
C. THE RAY PATH EQUATION	15
D. THE TREATMENT OF ATTENUATION IN RAY THEORY	18
E. REMARKS ON THE NATURE OF CLASSICAL RAY ACOUSTICS	19
1. Propagating discontinuities in the acoustic field	20
2. Ray theory as a high frequency approximation	21
IV ILLUSTRATIVE APPLICATIONS OF EXACT RAY THEORY	25
A. A COMPUTATIONAL PROCEDURE FOR TRACING EXACT RAYS	25
B. THE UNBOUNDED HOMOGENEOUS MEDIUM CASE	27
C. THE LINEAR SOUND SPEED CASE	28
D. A SMOOTH CAUSTIC SYSTEM	29
1. Classical ray analysis of the Kormilitsin profile	31
2. Ludwig's uniform asymptotic approximation	33
3. Frequency dependent ray analysis of a caustic	35
E. REMARKS ON THE NATURE OF EXACT RAY THEORY	38
F. PROPAGATION IN A WAVEGUIDE	40
1. Classical ray analysis of the harmonic oscillator waveguide	40
2. Normal mode representation of the field in a waveguide	41
3. Exact ray analysis of a refractive waveguide	44
4. Phase velocity	46
G. FRAUNHOFER DIFFRACTION	48
1. Radiation from a circular piston in a baffle	48

	<u>Page</u>
2. Diffraction of exact rays	49
H. BEAM DISPLACEMENT AND REFLECTIONS FROM A BOUNDARY	50
1. Reflection from a boundary	52
2. Frequency dependent ray representation of beam displacement	55
I. EXACT RAY THEORY AND MULTIPATHING	57
V CONCLUSION	59
REFERENCES	61

LIST OF FIGURES

Figure		Page
3.1	Conservation of energy in ray acoustics	13
4.1	Ray paths for the linear sound speed profile $c = az$	29
4.2	The Kormilitsin profile	30
4.3	Classical ray diagram for the Kormilitsin profile	32
4.4	Frequency dependent ray diagram for the Kormilitsin profile	36
4.5	Propagation loss curves for the Kormilitsin profile	37
4.6	The harmonic oscillator waveguide	41
4.7	Exact rays and classical rays in the harmonic oscillator waveguide	45
4.8	Level contours of the phase speed $c_{ph} = \omega/K$	47
4.9	The piston in a baffle	49
4.10	Beam displacement of a bottom reflected ray	51
4.11	Reflection from a rigid boundary	53
4.12	Beam displacement	56



Accession For	
NTIS CRA&I	<input checked="" type="checkbox"/>
DTIC TAB	<input type="checkbox"/>
Unannounced	<input type="checkbox"/>
Justification	
By	
Distribution/	
Availability Codes	
Dist	Avail and/or Special
A-1	

PREFACE

This report is an edited version of the dissertation submitted by Terry L. Foreman in partial fulfillment of the requirements for a Ph.D. degree in physics at The University of Texas at Austin. Portions of this work have been submitted for publication in the Journal of the Acoustical Society of America. This effort was supported by the Office of Naval Research through Contracts N00014-80-C-0490 and N00014-87-K-0346.

I. INTRODUCTION

Geometrical ray theory propagation models have consistently been among the most versatile and frequently used instruments of analysis in the underwater acoustician's inventory. The popularity of these models derives in part from certain computational advantages, particularly the ability to treat range dependent ocean environments and broadband sources with relative ease. But the success of the models is explained at least as much by their appeal to physical intuition—the easily conceptualized representation of the acoustic field by interacting rays of energy. Decades of experience with ray theory have brought a sense of familiarity with rays and how they behave. The behavior of the acoustic field in a complicated ocean environment can often be understood by studying a ray diagram, which may reveal the locations of convergence zones and shadow zones, regions where bottom interaction is important or unimportant, ducts where sound can propagate long distances with little attenuation, and myriad other details of the acoustical scene. Despite its well known shortcomings at treating caustics, bottom interaction, and weakly ducted propagation, ray theory provides much of the conceptual framework on which ideas about acoustic propagation are based. Physical intuition about the nature and behavior of rays has become quite ingrained.

Ray theory is at its best when used to track propagating discontinuities from impulsive sources. It is unsurpassed at computing arrival times and angles and amplitudes of disturbances as they advance into a quiescent medium. It is also quite good at high frequency acoustic field predictions for time harmonic sources, particularly when propagation distances are short. These have been the traditional domains of ray theory application. In recent years ray theory has been used increasingly to model long range, low frequency propagation, sometimes even in shallow water, and its weaknesses have begun to show. Yet the computational power and convenience of ray models and the insight they provide encourage their use even under these less than favorable circumstances.

The Helmholtz equation accurately describes the acoustic field in the farfield of a low frequency time harmonic source. The application of classical ray theory to the Helmholtz equation is based on a well known approximation. This dissertation is a study of an idealized ray theory in which the approximation has been circumvented. When the acoustic field can be computed accurately by some independent means, it then becomes possible to trace out the rays which would have resulted had the ray theory approximation not been made. The resulting exact ray diagrams provide new insight into the behavior of the acoustic field, and into the nature of classical ray theory and the ray theory approximation. This new ray theory therefore serves, not as a computational method, but as a new method for representing and displaying the acoustic field.

But the surprising outcome of numerical experiments is that exact ray diagrams bear little resemblance to their classical counterparts, even at high frequencies. Some

of the more significant differences are the following. (1) The ray path trajectories depend on the source frequency and configuration, and on the boundaries or radiation conditions. This is consistent with a geometrical representation of the solution to the Helmholtz equation, which is an elliptical partial differential equation. (2) The exact rays intrude into shadow zones impenetrable by classical rays. The infiltration of shadow zones is accomplished naturally, as a consequence of the fact that the field in the shadow zone, though small, is not nonexistent; the rays do not take on complex parameters in order to reach the shadow zone, as in some modified classical ray theories. (3) Exact ray theory predicts finite fields at caustics. (4) Last, and most significant, the exact rays never exhibit the multipathing which is the hallmark of classical ray theory. This item is closely related to the third. If it were possible for the exact rays to cross each other at all then there would inevitably be formed limiting surfaces—envelopes to the rays—where the rays cross tangentially. On these surfaces the ray tubes would pinch off and the transport equation would then predict nonphysical singularities in the acoustic field.

The development of exact ray theory begins in the next chapter with a brief derivation of the linear equations of oceanic acoustic wave propagation, primarily to establish the notation and conventions used in underwater acoustics and to identify the assumptions, simplifications, and approximations which underlie the work to follow. Since none of this material is really new, it seems appropriate to expedite the development by employing the somewhat abstract Lagrangian formalism for classical fields, as recommended by Morse and Feshbach,[1] to efficiently recapitulate and consolidate results obtained earlier by a more lengthy physical analysis. (Boyles' first chapter contains a comprehensive development.[2])

Chapter III contains a development and reassessment of classical ray theory which leads to the formulation of an exact ray theory. Hints begin to appear that the ray theory approximation, far from being an innocuous approximation of a small perturbative nature, is actually a quite drastic assumption. To invoke this approximation is to completely change the character of the ray paths.

A computational method is presented in Chapter IV which enables one to trace rays without resort to the ray theory approximation, provided a solution to the Helmholtz equation is already available. In other words, *given* a solution to the Helmholtz equation, the exact rays for that case can be computed parasitically. The remainder of Chapter IV is devoted to the exploration of the behavior of exact rays. Ray diagrams are constructed for several cases and contrasted with the classical ray diagrams. Here the consequences of the ray approximation become apparent. The differences between classical and exact ray theory are quite remarkable and much of the chapter is devoted to explaining the differences.

II. OCEANIC ACOUSTIC WAVE PROPAGATION

We seek equations which describe acoustic propagation in a compressible, stationary fluid. This is to be accomplished by determining a Lagrangian density for the fluid such that, when the time integral of the total Lagrangian is minimized according to Hamilton's principle, the equations of motion result. After imposing simplifying assumptions and approximations appropriate to the requirements of this dissertation, these equations will turn out to take the form of linear, scalar wave equations and Helmholtz equations.

A. THE LAGRANGIAN DENSITY

The Lagrangian density \mathcal{L} of a conservative system is the kinetic potential $\mathcal{T} - \mathcal{V}$, where \mathcal{T} is the kinetic energy density and \mathcal{V} the potential energy density. In the small signal approximation, the kinetic energy density of the fluid is simply

$$\mathcal{T} = \frac{1}{2}\rho_0\mathbf{v}\cdot\mathbf{v}, \quad (2-1)$$

where ρ_0 is the ambient density of the undisturbed fluid and \mathbf{v} is the particle velocity of an element of fluid, or fluid particle.

Finding the potential energy density is slightly more complicated. In order to proceed we use the fact that acoustic disturbances are perturbations of the medium from its undisturbed state. Accordingly, we express the total pressure p' as the sum of the ambient pressure p_0 and the excess pressure p due to the acoustic perturbation:

$$p'(\mathbf{r}, t) = p_0(\mathbf{r}) + p(\mathbf{r}, t);$$

but (in a somewhat inconsistent notation) we write the total density ρ in terms of the ambient density and the fractional change in density, σ , due to the acoustic disturbance:

$$\rho(\mathbf{r}, t) = \rho_0(\mathbf{r})[1 + \sigma(\mathbf{r}, t)]. \quad (2-2)$$

(We are now following Morse and Feshbach,[1] pp. 307-309.) When we speak of an acoustic disturbance it is understood that $\sigma \ll 1$ and that the acoustic pressure is much smaller than the bulk modulus ($p \ll \rho_0 c^2$). Notice that the ambient pressure and density, as written, may depend on position \mathbf{r} but not on time t . We are assuming a stationary medium for the purposes of this dissertation without claiming that temporal fluctuations are unimportant. In fact, the effects of fluctuations of the medium on acoustic propagation are a very active area of research.[3,4]

The potential energy stored in an infinitesimal volume of fluid is equal to the work done to compress the fluid from its original volume V_0 to its actual volume $V_0 - \Delta V$. Thus the potential energy density \mathcal{V} of the fluid is given by

$$\mathcal{V} = - \lim_{V_0 \rightarrow 0} \frac{1}{V_0} \int_{V_0}^{V_0 - \Delta V} p dV.$$

As the fluid is being compressed its volume decreases approximately according to $V = V_0(1 - \sigma)$. With a change of integration variable the expression for the potential energy becomes

$$\mathcal{V} = \int_0^\sigma p d\sigma.$$

Evidently we need the equation of state which governs the dependence of excess pressure on density in order to proceed. For most fluids, including seawater, the excess pressure is proportional to the fractional change in density in the small signal approximation:

$$p = \rho_0 c^2 \sigma,$$

where c is the speed of sound in the fluid. Then, with another change of integration variable, we finally obtain

$$\begin{aligned} \mathcal{V} &= \int_0^p \frac{p}{\rho_0 c^2} dp \\ &= \frac{p^2}{2\rho_0 c^2} \end{aligned} \quad (2-3)$$

as an expression for the the potential energy density.

With expressions (2-1) and (2-3) in hand for the kinetic and potential energy densities, we can write down a tentative form for the Lagrangian density:

$$\begin{aligned} \mathcal{L} &= \mathcal{T} - \mathcal{V} \\ &= \frac{1}{2} \left(\rho_0 \mathbf{v} \cdot \mathbf{v} - \frac{p^2}{\rho_0 c^2} \right). \end{aligned}$$

But this Lagrangian contains *four* field variables: the pressure p , and the three components of the particle velocity vector \mathbf{v} . The equations of motion for this system would be an unwieldy set of coupled vector equations.

We must pare down the number of field variables. Toward that end, if we neglect vorticity then we may introduce a scalar velocity potential ψ such that

$$\mathbf{v}(\mathbf{r}, t) = \nabla\psi, \quad (2-4)$$

and thereby replace the vector field \mathbf{v} with the scalar ψ . This approximation is almost always valid in underwater acoustics. Moreover, Lighthill[5] points out that, in linear theory, $\mathbf{v} = \nabla\psi$ is the irrotational part of the total velocity field and does not interact with any steady rotational flow field. We will make the further assumption that there is *no* steady flow field. This approximation is usually well justified in underwater acoustics, where typical current and eddy flow speeds are ~ 1 m/s, while the sound speed has a nominal value of 1500 m/s.

With the velocity potential thus defined, the Lagrangian density becomes

$$\mathcal{L} = \frac{1}{2} \left(\rho_0 \nabla\psi \cdot \nabla\psi - \frac{p^2}{\rho_0 c^2} \right), \quad (2-5)$$

which still contains two field variables, namely ψ and p . We will eliminate p in favor of ψ , although some researchers prefer to work with the pressure and hence do the opposite. In the absence of viscosity and external forces, the pressure and particle velocity are related by (see Morse and Feshbach,[1] pp. 151-160, 308)

$$\rho_0 \frac{\partial \mathbf{v}}{\partial t} = -\nabla p. \quad (2-6)$$

By equating gradients in Eq. (2-6) and the time derivative of Eq. (2-4), we see that

$$p = -\rho_0 \frac{\partial \psi}{\partial t} \quad (2-7)$$

to within a constant, which is set to zero. The Lagrangian (2-5) can now be written in the desired form

$$\mathcal{L} = \frac{\rho_0}{2} \left[\nabla \psi \cdot \nabla \psi - \frac{1}{c^2} \left(\frac{\partial \psi}{\partial t} \right)^2 \right], \quad (2-8)$$

with ψ as the only remaining field variable.

B. THE ACOUSTIC WAVE EQUATION

According to Hamilton's principle for a conservative system, the system will move so that the time average of the kinetic potential is an extremum (usually a minimum). The equations of motion which satisfy Hamilton's principle are the Euler-Lagrange equations. We are now prepared to generate a wave equation by substituting the Lagrangian density (2-8) in the Euler-Lagrange equation

$$\frac{d}{dt} \left(\frac{\partial \mathcal{L}}{\partial \left(\frac{\partial \psi}{\partial t} \right)} \right) + \frac{d}{dx_i} \left(\frac{\partial \mathcal{L}}{\partial \left(\frac{\partial \psi}{\partial x_i} \right)} \right) - \frac{\partial \mathcal{L}}{\partial \psi} = 0.$$

The Lagrangian is to be regarded as an explicit function of time, the coordinates, the field variable, and the derivatives of the field variable with respect to time and the coordinates: $\mathcal{L} = \mathcal{L}(t, x_i, \psi, \partial \psi / \partial t, \partial \psi / \partial x_i)$. The summation convention on repeated indices is assumed, so that, for example, the particle velocity can be expressed as

$$\begin{aligned} \mathbf{v} &= \nabla \psi \\ &= \left(\mathbf{e}_x \frac{\partial}{\partial x} + \mathbf{e}_y \frac{\partial}{\partial y} + \mathbf{e}_z \frac{\partial}{\partial z} \right) \psi \\ &= \mathbf{e}_i \frac{\partial \psi}{\partial x_i}, \end{aligned}$$

and $\nabla^2 \psi$ can be written as $\partial^2 \psi / \partial x_i \partial x_i$. In this notation the Lagrangian (2-8) takes the form

$$\mathcal{L} = \frac{\rho_0}{2} \left[\frac{\partial \psi}{\partial x_i} \frac{\partial \psi}{\partial x_i} - \frac{1}{c^2} \left(\frac{\partial \psi}{\partial t} \right)^2 \right].$$

Then the equation of motion turns out to be

$$\begin{aligned} 0 &= \frac{d}{dt} \left(\frac{\partial \mathcal{L}}{\partial \left(\frac{\partial \psi}{\partial t} \right)} \right) + \frac{d}{dx_i} \left(\frac{\partial \mathcal{L}}{\partial \left(\frac{\partial \psi}{\partial x_i} \right)} \right) - \frac{\partial \mathcal{L}}{\partial \psi} \\ &= \frac{\partial}{\partial t} \left(-\frac{\rho_0}{c^2} \frac{\partial \psi}{\partial t} \right) + \frac{\partial}{\partial x_i} \left(\rho_0 \frac{\partial \psi}{\partial x_i} \right) \\ &= \rho_0 \left(\frac{\partial^2 \psi}{\partial x_i \partial x_i} + \frac{1}{\rho_0} \frac{\partial \rho_0}{\partial x_i} \frac{\partial \psi}{\partial x_i} - \frac{1}{c^2} \frac{\partial^2 \psi}{\partial t^2} \right), \end{aligned}$$

or

$$\nabla^2 \psi + \frac{\nabla \rho_0}{\rho_0} \cdot \nabla \psi = \frac{1}{c^2} \frac{\partial^2 \psi}{\partial t^2}, \quad (2-9)$$

which is the desired wave equation. Because of the presence of the density gradient term, Eq. (2-9) will be referred to as the modified wave equation.¹

C. THE HELMHOLTZ EQUATION

The Fourier transform $\Psi(\mathbf{r}, \omega)$ of $\psi(\mathbf{r}, t)$ is defined by

$$\Psi = \frac{1}{\sqrt{2\pi}} \int_{-\infty}^{\infty} \psi e^{i\omega t} dt.$$

Because the modified wave equation (2-9) is linear, Ψ will satisfy the Fourier transform of Eq. (2-9), namely

$$\nabla^2 \Psi + \frac{\nabla \rho_0}{\rho_0} \cdot \nabla \Psi + k^2 \Psi = 0, \quad (2-10)$$

which is the modified Helmholtz equation. The wave number k is defined by

$$k = \frac{\omega}{c}.$$

Equation (2-10) can be rendered in a more familiar form which lacks the density gradient term by defining a new field variable:

$$q = \rho_0^{1/2} \Psi. \quad (2-11)$$

After substituting the expression (2-11) for q in Eq. (2-10) we get the Helmholtz equation²

$$\nabla^2 q + \kappa^2 q = 0, \quad (2-12)$$

¹One might object that the derivation of Eq. (2-9) is inconsistent in that external forces, here neglected, must be present in order to create a density gradient. Indeed, if the external force \mathbf{F} is obtained from a potential V by $\mathbf{F} = -\nabla V$, then Eq. (2-7) should be modified to $p = -(\rho_0 \partial \psi / \partial t + V)$. But it is easily verified that, for time independent forces, the resulting extra terms in the Lagrangian density have no effect on the wave equation.

²Universal agreement on equation names is lacking, as usual. The Helmholtz equation (2-12) is also called the reduced wave equation. Morse and Feshbach, whose development we had been following, would call Eq. (2-12) a Helmholtz equation if κ were a constant, and a (time independent) Schrödinger equation otherwise. The distinction is crucial to their cataloging of the coordinate systems in which the Helmholtz equation (in their sense) is separable. That distinction is irrelevant here and we refer to Eq. (2-12) as a Helmholtz equation because it has the right form.

where

$$\kappa^2 = k^2 + \frac{1}{4} \frac{\nabla \rho_0}{\rho_0} \cdot \frac{\nabla \rho_0}{\rho_0} - \frac{1}{2} \frac{\nabla^2 \rho_0}{\rho_0}.$$

However, it is rarely necessary in practical applications to make this transformation; the density gradient term in Eq. (2-10) can usually be ignored. Rutherford and Hawker[6] investigated the sensitivity to variations in the density gradient of solutions to the depth separated modified Helmholtz equation

$$\frac{d^2 u}{dz^2} + \frac{1}{\rho_0} \frac{d\rho_0}{dz} \frac{du}{dz} + (k^2 - \gamma^2)u = 0, \quad (2-13)$$

where γ^2 is the separation constant. They conducted the sensitivity study for various sediment layers underlying the ocean bottom and found that solutions to Eq. (2-13) were quite insensitive to the details of the density profile *within* sediment layers; they were, however, sensitive to the *ratios* of the densities of two sediment layers at their common interface. Thus they determined that the density gradient term could be dropped from Eq. (2-13) provided that the correct density ratios at interfaces were retained. Moreover, typical density gradients in the sediments often exceed those in the water by an order of magnitude; if the density gradient term is ignorable in sediments then *a fortiori* it is ignorable in the water column.

1. Sources and boundary conditions

We will only be concerned with point, time harmonic sources with time dependence $e^{-i\omega t}$. Usually, we will be concerned with finding the Green function Ψ_G which satisfies the inhomogeneous modified Helmholtz equation

$$\nabla^2 \Psi_G + k^2 \Psi_G = -\delta(\mathbf{r} - \mathbf{r}_0)$$

for a source located at \mathbf{r}_0 .

At propagation ranges many times the depth of the ocean, acoustic energy is effectively trapped in the channel formed by the surface and bottom of the ocean, and the ocean begins to take on the properties of a waveguide. As is often the case with propagation in a waveguide, rough periodicities in the acoustic field are frequently evident. Cycle distances of 50 km or so are typical. Sound waves are refracted by inhomogeneities in the medium, and the energy propagation paths predicted by ray theory become very complicated at ranges beyond a cycle distance. Failures of the ray theory approximation begin to manifest at ranges beyond a cycle distance and at frequencies low enough (below 5000 Hz) to propagate to such distances without being completely absorbed.

The focus of this investigation is on the exact ray theory developed in Chapters III and IV rather than the problems of modeling acoustic propagation in difficult ocean environments. It is desirable to illustrate the theory using the simplest possible idealizations of the oceanic waveguide. With this in mind, the simplified boundary and radiation conditions described below will usually suffice.

The atmosphere above the sea surface is so tenuous compared to the water that very little acoustic energy passes from the water into the air. It is sufficient to idealize the air-water interface as a planar pressure release perfect reflector at which the acoustic field vanishes. One should note, however, that considerable research is underway on the effects of scattering from surface waves and polar ice caps.

Similarly, even though acoustic interaction with the ocean bottom is also an important area of research, it suffices here to treat the bottom as a plane lying parallel to the surface.

The acoustic field is considered to consist entirely of outgoing waves. In a horizontally stratified waveguide this leads to the requirement that the acoustic field satisfy the Sommerfeld radiation condition

$$\lim_{r \rightarrow \infty} \sqrt{r} \left(\frac{\partial \psi}{\partial r} - i\psi k(z) \right) = 0$$

in cylindrical coordinates where r is horizontal range along the waveguide and z is depth below the surface.

2. Attenuation

It is convenient to define a complex velocity potential φ for a time harmonic source by

$$\varphi = \Psi e^{-i\omega t}, \quad (2-14)$$

where

$$\psi = \text{Re } \varphi. \quad (2-15)$$

It can be shown by substitution that φ satisfies the acoustic wave equation (2-9) for sources with time dependence $e^{-i\omega t}$. Moreover, φ also satisfies the modified Helmholtz equation:

$$\nabla^2 \varphi + \frac{\nabla \rho_0}{\rho_0} \cdot \nabla \varphi + k^2 \varphi = 0; \quad (2-16)$$

in fact, the modified Helmholtz equation can be *derived* by substituting φ in the modified wave equation.

We now exploit the property of the Lagrange formulation of classical fields that all Lagrangian densities which generate the same equations of motion are equivalent³ (though not all Lagrangians have the same physical content). Here, a Lagrangian density which generates the modified Helmholtz equation (2-16) is

$$\mathcal{L} = \rho_0 (\nabla \varphi \cdot \nabla \varphi^* - k^2 \varphi \varphi^*), \quad (2-17)$$

³Actually, this statement is strictly true only when the Lagrangian is invariant to coordinate transformations. We avoid these complications by staying with Cartesian coordinates while working out the Euler-Lagrange equations. Once the equations of motion have been derived they can be rewritten for any desired coordinate system.

where there are now *two* independent field variables, φ and the conjugate field φ^* . Substitution of the Lagrangian (2-17) in the Euler-Lagrange equation, with φ^* as the field variable, produces the modified Helmholtz equation

$$\nabla^2 \varphi + \frac{\nabla \rho_0}{\rho_0} \cdot \nabla \varphi + k^2 \varphi = 0.$$

Similarly, the Euler-Lagrange equation with respect to φ is

$$\nabla^2 \varphi^* + \frac{\nabla \rho_0}{\rho_0} \cdot \nabla \varphi^* + k^2 \varphi^* = 0,$$

and the conjugate field φ^* is thus seen also to satisfy the modified Helmholtz equation.

Only for conservative systems will the Lagrange function density take the form $\mathcal{T} - \mathcal{V}$. Having thus excluded dissipative mechanisms at the outset of our development by using the Lagrangian formulation, we will now readmit them by a subterfuge. The trick is to add an extra term to the Lagrangian (2-17):

$$\mathcal{L} = \rho_0 \left[\nabla \varphi \cdot \nabla \varphi^* - k^2 \varphi \varphi^* + \frac{1}{2} \alpha \left(\varphi^* \frac{\partial \varphi}{\partial t} - \varphi \frac{\partial \varphi^*}{\partial t} \right) \right],$$

which will cause the conjugate field φ^* to gain in amplitude as rapidly as the field φ attenuates, thereby preserving the total energy of the system as a constant and thus permitting the continued use of the Lagrangian formulation (it is understood that these gains and losses take place in space, not time). The Euler-Lagrange equations are

$$\nabla^2 \varphi + \frac{\nabla \rho_0}{\rho_0} \cdot \nabla \varphi + k^2 \varphi - \alpha \frac{\partial \varphi}{\partial t} = 0 \quad (2-18)$$

and

$$\nabla^2 \varphi^* + \frac{\nabla \rho_0}{\rho_0} \cdot \nabla \varphi^* + k^2 \varphi^* + \alpha \frac{\partial \varphi^*}{\partial t} = 0. \quad (2-19)$$

Since $\varphi = \Psi e^{-i\omega t}$, the field equations (2-18) and (2-19) become

$$\nabla^2 \Psi + \frac{\nabla \rho_0}{\rho_0} \cdot \nabla \Psi + (k^2 + i\alpha\omega) \Psi = 0 \quad (2-20)$$

and

$$\nabla^2 \Psi^* + \frac{\nabla \rho_0}{\rho_0} \cdot \nabla \Psi^* + (k^2 - i\alpha\omega) \Psi^* = 0, \quad (2-21)$$

now in terms of Ψ and Ψ^* again. Only the solution to Eq. (2-20) is of direct physical interest, for Ψ will suffer the desired attenuation while Ψ^* , the solution to Eq. (2-21), will grow to compensate.

Morse and Feshbach recommend this *ad hoc* device for introducing dissipation into the Lagrangian only when the loss mechanisms are not well understood. The mechanisms of attenuation in the ocean are actually understood reasonably well[7]

but are also rather complicated; to treat them thoroughly would take us too far afield. Instead we embrace equation (2-20), which is commonly modified to

$$\nabla^2 \Psi + \frac{\nabla \rho_0}{\rho_0} \cdot \nabla \Psi + (k + ia)^2 \Psi = 0 \quad (2-22)$$

(valid for $a \ll k$, with $a = \frac{1}{2}\alpha c$), as a successful phenomenological model of time harmonic propagation in a slightly lossy ocean. The attenuation $a(\mathbf{r}, \omega)$ is usually determined empirically and incorporates the effects of thermoviscous and relaxation loss mechanisms (absorption) as well as bulk scattering losses. It has dimensions of nepers per unit length.

The remainder of this dissertation is chiefly concerned with constructing exact ray diagrams for various solutions to the lossy modified Helmholtz equation (2-22) and with using exact ray theory to exhibit the behavior of the acoustic field.

III. REVIEW OF RAY THEORY

This chapter begins with what is essentially the Sommerfeld development of ray theory,[8] perhaps the simplest of several alternative derivations. Moreover, the Sommerfeld development directly addresses the application of ray theory to the Helmholtz equation and it requires only one approximation, which is clearly identified. The methodology and order of presentation given here are somewhat unconventional in order to advance a view of classical ray acoustics as an approximation to an exact ray theory in which the ray trajectories depend on the configuration and radiating frequency of the time harmonic sources.¹ Ray theory in the traditional view is the high frequency limit of an asymptotic expansion in which the ray paths are independent of frequency. The two viewpoints are not incompatible and a proof of the latter claim is also given.

A. THE RAY PATH AND TRANSPORT EQUATIONS

We will obtain the eikonal and transport equations of ray acoustics by further manipulation of the Lagrangian, and from these we will derive the ray path equation and an energy conservation law.

A Lagrangian density (2-17) which yields the modified Helmholtz equation in a lossless medium was found in Sec. II.C.2 to be

$$\mathcal{L} = \rho_0(\nabla\varphi \cdot \nabla\varphi^* - k^2\varphi\varphi^*),$$

which becomes

$$\mathcal{L} = \rho_0(\nabla\Psi \cdot \nabla\Psi^* - k^2\Psi\Psi^*) \quad (3-1)$$

upon using the defining relation $\varphi = \Psi e^{-i\omega t}$. Henceforth we will assume that the density dependence of the Helmholtz equation has been abolished, either by a change of variables or by simply ignoring it, as discussed in Sec. II.C. Then the Lagrangian (3-1) may be replaced by

$$\mathcal{L}' = \nabla\Psi \cdot \nabla\Psi^* - k^2\Psi\Psi^*, \quad (3-2)$$

as one may verify by substituting \mathcal{L}' in the Euler-Lagrange equation and showing that the Helmholtz equation

$$\nabla^2\Psi + k^2\Psi = 0 \quad (3-3)$$

is thereby recovered.

A Lagrangian density which leads to the ray theoretical formulation of the Helmholtz equation is obtained by writing Ψ explicitly in terms of its real amplitude A and phase Φ :

$$\Psi = Ae^{i\Phi},$$

¹A somewhat similar theoretical development by Floyd[9] does not retain the concept of a geometrical energy conservation law, which is a central feature of the ray theory described here.

and substituting in the Lagrangian (3-2) to produce a new Lagrangian

$$\begin{aligned}\mathcal{L} &= (\nabla A + iA\nabla\Phi) \cdot (\nabla A - iA\nabla\Phi) - k^2 A^2 \\ &= \nabla A \cdot \nabla A + A^2 \nabla\Phi \cdot \nabla\Phi - k^2 A^2.\end{aligned}$$

When the Euler-Lagrange machinery is applied to the new Lagrangian it generates two coupled equations for the new field variables A and Φ . One of the Euler-Lagrange equations is

$$\begin{aligned}0 &= \frac{d}{dx_i} \left(\frac{\partial \mathcal{L}}{\partial \left(\frac{\partial A}{\partial x_i} \right)} \right) - \frac{\partial \mathcal{L}}{\partial A} \\ &= 2 \left(\frac{\partial^2 A}{\partial x_i \partial x_i} - A \nabla\Phi \cdot \nabla\Phi + k^2 A \right),\end{aligned}$$

or

$$\nabla\Phi \cdot \nabla\Phi = k^2 + \frac{\nabla^2 A}{A}. \quad (3-4)$$

Equation (3-4) will be referred to as the *exact* eikonal equation in order to distinguish it from the more familiar eikonal equation of classical ray acoustics, which will appear later. Likewise, Φ will be called the exact eikonal.

The other Euler-Lagrange equation is

$$\begin{aligned}0 &= \frac{d}{dx_i} \left(\frac{\partial \mathcal{L}}{\partial \left(\frac{\partial \Phi}{\partial x_i} \right)} \right) - \frac{\partial \mathcal{L}}{\partial \Phi} \\ &= 2 \left(2A \frac{\partial A}{\partial x_i} \frac{\partial \Phi}{\partial x_i} + A^2 \frac{\partial^2 \Phi}{\partial x_i \partial x_i} \right),\end{aligned}$$

or

$$2 \frac{\nabla A}{A} \cdot \nabla\Phi + \nabla^2 \Phi = 0, \quad (3-5)$$

which is the transport equation.

The eikonal equation leads to an equation for the paths of acoustic energy propagation, or ray paths. The transport equation leads to a geometrical energy conservation law in a form useful for the calculation of the sound intensity at any point along a ray path. The eikonal and transport equations are coupled, first order in $\nabla A/A$ and $\nabla\Phi$, and nonlinear; they are entirely equivalent to the second order, linear Helmholtz equation (3-3). They may also be obtained, as in the Sommerfeld development, by direct substitution of $Ae^{i\Phi}$ in the Helmholtz equation.

To bring the concept of rays into the development, first define the unit vector \mathbf{t} to be the outward normal to a surface of constant phase Φ at the point \mathbf{r} , and further *define* \mathbf{t} to be the tangent vector to the ray path at \mathbf{r} . (In some ray theories, particularly those applicable to moving media, the ray paths are *not* necessarily perpendicular to the surfaces of constant phase.) It is also convenient to define the wave vector \mathbf{K} by

$$\mathbf{K} = \nabla\Phi,$$

so that $\mathbf{K} = K\mathbf{t}$. The ray path trajectory is the solution to $d\mathbf{r}/ds = \mathbf{t}$, where ds is the element of ray path length. The exact eikonal equation then becomes

$$\mathbf{K}^2 = k^2 + \frac{\nabla^2 A}{A}. \quad (3-6)$$

The transport equation (3-5) may be expressed as a vanishing divergence:

$$\nabla \cdot (A^2 \mathbf{K}) = 0. \quad (3-7)$$

B. CONSERVATION OF ENERGY

Departing slightly from the usual order of the Sommerfeld development, we will follow up on the discussion of the transport equation before deriving the ray path equation. The formulation of the transport equation (3-7) as a vanishing divergence suggests applying Gauss's theorem. Accordingly, let S be the closed surface formed by a tube of rays and the intersection of the tube with two surfaces of constant phase, S_1 and S_2 , as shown in Fig. 3.1. Let V be the volume enclosed by S . Then by Gauss's

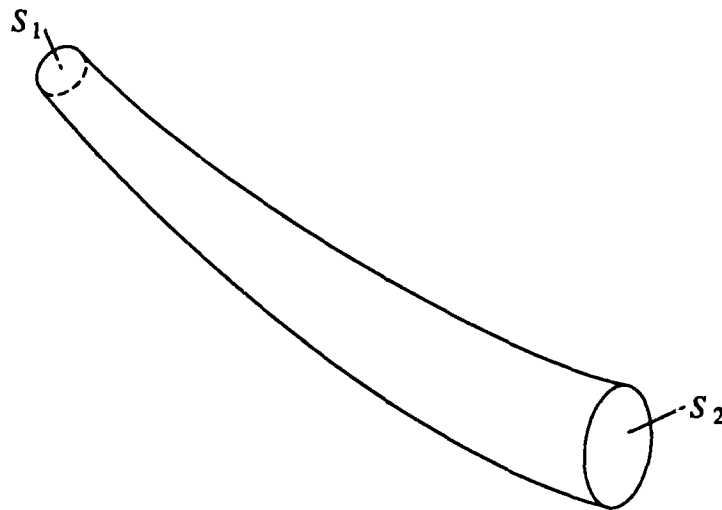


FIGURE 3.1 CONSERVATION OF ENERGY IN RAY ACOUSTICS. THE TIME AVERAGED ENERGY FLUX THROUGH THE SURFACE OF CONSTANT PHASE, S_1 , EQUALS THE FLUX THROUGH S_2 .

theorem,

$$\int_V \nabla \cdot (A^2 \mathbf{K}) dV = \int_S A^2 \mathbf{K} \cdot \mathbf{n} dS = 0, \quad (3-8)$$

where \mathbf{n} is the outward unit vector normal to S . The only contributions to the integral are from the end caps S_1 and S_2 since $\mathbf{K} \cdot \mathbf{n} = 0$ by definition on the sides of S formed by the ray tube. And since \mathbf{K} is tangential to the ray path, then also by definition,

$$\mathbf{n} = \begin{cases} -\mathbf{t} & \text{on } S_1 \\ \mathbf{t} & \text{on } S_2 \end{cases}. \quad (3-9)$$

Using Eq. (3-9) in Eq. (3-8) yields

$$\begin{aligned} 0 &= \int_S A^2 \mathbf{K} \cdot \mathbf{n} dS \\ &= \int_{S_2} A^2 \mathbf{K} \cdot \mathbf{t} dS - \int_{S_1} A^2 \mathbf{K} \cdot \mathbf{t} dS, \end{aligned}$$

or

$$\int_{S_1} A^2 K dS = \int_{S_2} A^2 K dS, \quad (3-10)$$

which is the integral form of the transport equation.

The significance of Eq. (3-10) becomes apparent upon identifying $\frac{1}{2}\rho_0\omega A^2 K$ as the time averaged acoustic intensity, or energy flux. The intensity of a classical field has dimensions of force per unit area times velocity. We therefore expect, by dimensional analysis, that the instantaneous intensity \mathbf{J} is given by

$$\mathbf{J} = p\mathbf{v} \quad (3-11)$$

since pressure has units of force per unit area. (A complete derivation is given by Boyles,[2] pp. 30-34.) The energy flux \mathbf{J} is sometimes called the Poynting vector, although that term is more commonly applied to the analogous electromagnetic field intensity.

In terms of the complex velocity potential $\Psi e^{-i\omega t}$, the particle velocity (2-4) is

$$\mathbf{v} = \text{Re}(\nabla\Psi e^{-i\omega t}) \quad (3-12)$$

and the pressure (2-7) is

$$\begin{aligned} p &= -\rho_0 \text{Re}\left[\frac{\partial}{\partial t}(\Psi e^{-i\omega t})\right] \\ &= -\rho_0\omega \text{Im}(\Psi e^{-i\omega t}). \end{aligned} \quad (3-13)$$

Then, using $\Psi = Ae^{i\Phi}$ and Eqs. (3-12) and (3-13) for \mathbf{v} and p , the expression for the intensity (3-11) becomes

$$\mathbf{J} = \rho_0\omega A^2 \left(\nabla\Phi \sin^2(\Phi - \omega t) - \frac{\nabla A}{A} \sin(\Phi - \omega t) \cos(\Phi - \omega t) \right).$$

The time average of the intensity, $\langle \mathbf{J} \rangle$, is obtained by integrating \mathbf{J} over the period T :

$$\langle \mathbf{J} \rangle = \frac{1}{T} \int_0^T \mathbf{J} dt,$$

with $T = \omega/2\pi$. The integral is easily calculated and the result takes the form

$$\langle \mathbf{J} \rangle = \frac{1}{2}\rho_0\omega A^2 \mathbf{K} \quad (3-14)$$

if one uses the definition $\nabla\Phi = \mathbf{K}$. Thus the time averaged intensity is directed along the ray path,² although the instantaneous flux vector points in the direction of \mathbf{v} , which is time dependent and generally not parallel to the ray path.

In view of Eq. (3-14), the integral form of the transport equation (3-10) can be written as

$$\int_{S_1} \langle \mathbf{J} \rangle \cdot d\mathbf{S} = \int_{S_2} \langle \mathbf{J} \rangle \cdot d\mathbf{S},$$

which is

$$\int_{S_1} \langle J \rangle dS = \int_{S_2} \langle J \rangle dS. \quad (3-15)$$

This is an energy conservation law in geometrical form. It states that all of the energy flux which passes through the surface S_1 also passes through S_2 . The existence of such a law helps to explain the popularity and versatility of ray theory.

We have established not only that the ray paths are physically meaningful in that they are the trajectories of energy propagation (although we have not yet seen how to compute the trajectories), but we also have an intuitively appealing picture of how the intensity varies along a ray path as the ray tube expands and contracts. The energy conservation law (3-15) also readily lends itself to computation. Ray theory is unique in its ability to present a qualitative and informative view of energy propagation and to permit straightforward calculation of the acoustic field.

It should be emphasized that no approximations have been made up to this point; the geometrical energy conservation law (3-15) is *not* a ray theory approximation, as is sometimes stated; it does not arise from the "neglect of diffraction," or the "local approximation of the field by a plane wave," or any other classical ray theory approximation. Moreover, Eqs. (3-10) and (3-15) are fully applicable to finite sources; nothing in the development requires that the ray tubes include only infinitesimal volumes. We will, in the next section, resort to an approximation in order to be able to compute the ray trajectories, but this approximation is made in the ray path equation, not the transport equation.

C. THE RAY PATH EQUATION

We have shown that there are trajectories along which sound propagates. An equation for these paths may be obtained by computing the gradient of K^2 :

$$\begin{aligned} K^2 &= \mathbf{K} \cdot \mathbf{K}; \\ 2K \nabla K &= 2(\mathbf{K} \cdot \nabla) \mathbf{K} + 2\mathbf{K} \times (\nabla \times \mathbf{K}). \end{aligned}$$

²It can be shown (see Boyles[2]) that the result (3-14) can also be found from $\langle \mathbf{J} \rangle = \frac{1}{2} \text{Re}(P\mathbf{V}^*)$ for time harmonic fields, where the complex particle velocity is defined by $\mathbf{V} = \nabla\varphi = \nabla\Psi e^{-i\omega t}$ and the complex pressure is given by $P = -\rho_0 \partial\varphi/\partial t = i\rho_0\omega\Psi e^{-i\omega t}$.

Since $\nabla \times \mathbf{K} = \nabla \times \nabla \Phi = 0$, this simplifies to

$$\begin{aligned}\nabla K &= \left(\frac{\mathbf{K}}{K} \cdot \nabla \right) \mathbf{K} \\ &= \left(\frac{d\mathbf{r}}{ds} \cdot \nabla \right) \mathbf{K} \\ &= \frac{d\mathbf{K}}{ds},\end{aligned}$$

or

$$\frac{d}{ds} \left(K \frac{d\mathbf{r}}{ds} \right) = \nabla K. \quad (3-16)$$

Equation (3-16) is a ray path equation; its solutions are the energy conserving ray path trajectories described in the previous section.

It is worth reemphasizing that no approximations have yet been made; the Helmholtz equation has been recast in what might be termed an exact ray theoretical formulation. The simultaneous solution of the ray path equation (3-16) and the transport equation (3-7) would yield A and Φ and thus determine Ψ , the solution to the Helmholtz equation.

The difficulty is that solving the ray path equation requires knowledge of K , which in turn requires knowledge of A , as may be seen by examining the eikonal equation (3-6). And, of course, the ray paths must be known in order to solve the transport equation for A . We have come full circle. In principle, the exact eikonal and transport equations can be solved simultaneously, for example by numerical methods, but that will usually prove more difficult than solving the original Helmholtz equation.

Yet this "exact ray theory" nevertheless proves useful, not as a general purpose computational procedure, but as an investigative and display technique. When the solution to the Helmholtz equation is available by independent means then the cycle described in the last paragraph can be broken; *given* the solution to the Helmholtz equation one could compute A and then K and proceed to trace rays. (A more practical computational method for tracing exact rays is explained in the next chapter.) *Exact ray diagrams are a new alternative to propagation loss curves and intensity plots as a means of displaying and analyzing the acoustic field.* As we shall see in Chapter IV, exact ray diagrams usually differ strikingly from their classical counterparts.

The source of the difficulty with exact ray theory as a computational method is that the eikonal and transport equations are coupled: one cannot determine K exactly without first knowing A . In classical ray acoustics the desired decoupling is achieved by resorting to an approximation. If $\nabla^2 A/A \ll k^2$, then by neglecting $\nabla^2 A/A$ in the eikonal equation one obtains

$$K \approx k. \quad (3-17)$$

This is the classical ray theory approximation; it is the *only* approximation required to obtain classical ray acoustics, but it has far-reaching consequences.

It can be shown that the ray theory approximation will fail wherever the sound speed gradient changes significantly over a wavelength.[10] In underwater acoustics, such rapid variations can occur at fronts where cold and warm ocean waters meet, or when one attempts to perform low frequency ray calculations in the ocean bottom sediments. However, the approximation is also observed to fail regularly even when the ocean environment harbors no regions of rapid sound speed variation at all. Regions where the acoustic field amplitude undergoes rapid spatial variations (i.e., where $\nabla^2 A/A \sim k^2$ and the approximation is invalid by definition) are simply not always, or even often, collocated with or causally related to regions of rapid sound speed variations. These problematical regions include the vicinity of caustics (to be discussed at length in Chapter IV) and ocean surface ducts. Because of their ubiquity, these regions are far more troublesome to the routine use of ray theory than rare pathological features in the sound speed field.

Nevertheless, the ray theory approximation does decouple the eikonal and transport equations and thus removes the dependence of K on A . The ray path equation (3-16) then becomes

$$\frac{d}{ds} \left(k \frac{dr}{ds} \right) = \nabla k.$$

Since k is a known function of the frequency and sound speed one can solve the ray path equation and trace rays at will.

If we define an index of refraction n in terms of a constant reference sound speed³ c_0 :

$$n = c_0/c,$$

then $k = \omega n/c_0$ and the ray path equation becomes

$$\frac{d}{ds} \left(n \frac{dr}{ds} \right) = \nabla n, \quad (3-18)$$

which is perhaps the most familiar form of the classical ray path equation. In the ray theory approximation the transport equation becomes

$$\nabla \cdot \left(A^2 n \frac{dr}{ds} \right) = 0,$$

and is generally restricted to infinitesimal ray tubes for reasons which will become apparent later.

Most fluids, including seawater, are only very slightly dispersive; that is, the dependence of c or n on ω is negligible for our purposes. The classical ray paths, which are solutions to Eq. (3-18), are consequently independent of frequency.⁴

³The natural choice for the value of c_0 in optics is the speed of light in a vacuum. There is no analogous preferred reference sound speed in acoustics and many workers simply use $1/c$, sometimes called the "slowness," in place of n .

⁴When attenuation is taken into consideration the wave number k or, equivalently, the sound speed takes on a small imaginary part which is frequency dependent. A lossy medium is therefore also a dispersive medium.

By contrast, K is a complicated function of frequency because of its dependence on A , which is sensitive to frequency. The ray trajectories which are solutions to the exact ray path equation (3-16), and which are the paths of acoustic energy propagation, are inherently frequency dependent. We generally expect dispersion in an inhomogeneous medium even if the sound speed itself is not an explicit function of frequency.

D. THE TREATMENT OF ATTENUATION IN RAY THEORY

Let us see how the inclusion of attenuation modifies the ray theory analysis presented earlier for lossless media. It was shown in Sec. II.C.2 that, for a source with time dependence $e^{-i\omega t}$, one may account for the effects of attenuation to first order by adding a small imaginary part to k ; that is, $k \rightarrow k + ia$. Accordingly, we will seek a first order perturbative solution to the lossy Helmholtz equation by expanding about the solution to the lossless equation in the small parameter a , with ϵ as an ordering parameter.

Let $\Psi_0 = Ae^{i\Phi}$ denote the solution to the lossless Helmholtz equation $\nabla^2\Psi_0 + k^2\Psi_0 = 0$ (recall that A and Φ are real). The lossy Helmholtz equation is written as

$$\nabla^2\Psi + (k + i\epsilon a)^2\Psi = 0, \quad (3-19)$$

and the solution proposed for it as

$$\Psi = \Psi_0 e^{-\epsilon\beta}. \quad (3-20)$$

The factor $e^{-\epsilon\beta}$ accounts for the expected spatial damping of the field amplitude; it was written in this form in anticipation of finding that $\beta = \int a ds$, which gives the usual path integral correction for attenuation in ray theory.

After substituting the expression (3-20) for Ψ in Eq. (3-19) and linearizing in ϵ , one obtains

$$\begin{aligned} \nabla^2\Psi_0 + k^2\Psi_0 \\ - \epsilon[\beta(\nabla^2\Psi_0 + k^2\Psi_0) + 2\nabla\Psi_0 \cdot \nabla\beta + \Psi_0\nabla^2\beta - 2i\Psi_0ak] = 0. \end{aligned}$$

The term of order ϵ^0 and the parenthetical expression in the term of order ϵ^1 simply reaffirm the Helmholtz equation and vanish identically, leaving

$$2\nabla\Psi_0 \cdot \nabla\beta + \Psi_0\nabla^2\beta = 2i\Psi_0ak. \quad (3-21)$$

But

$$\nabla\Psi_0 = \Psi_0 \left(\frac{\nabla A}{A} + iK \frac{d\mathbf{r}}{ds} \right),$$

which, in the ray theory approximation $\nabla A/A \ll k$, simplifies to

$$\nabla\Psi_0 = i\Psi_0k \frac{d\mathbf{r}}{ds}. \quad (3-22)$$

Substitution of Eq. (3-22) for $\nabla\Psi_0$ in Eq. (3-21) gives

$$2ik\frac{d\mathbf{r}}{ds}\cdot\nabla\beta + \nabla^2\beta = 2iak. \quad (3-23)$$

Since all of the variables in Eq. (3-23) are explicitly real, the real and imaginary parts of Eq. (3-23) must vanish separately, leaving a pair of coupled equations:

$$\nabla^2\beta = 0, \quad (3-24)$$

and

$$\frac{d\mathbf{r}}{ds}\cdot\nabla\beta = a. \quad (3-25)$$

By using the operator identity $d\mathbf{r}/ds\cdot\nabla = d/ds$, Eq. (3-25) can be written as

$$\frac{d\beta}{ds} = a,$$

or, upon integrating with respect to path length,

$$\beta = \int_0^s a ds'. \quad (3-26)$$

It is standard practice in ray calculations to treat attenuation by applying the formula

$$\Psi = Ae^{-\beta}e^{i\Phi},$$

where β is given by the path integral (3-26). Such path integrals are easy to compute numerically.

Equation (3-24) is essentially an assertion that β is slowly varying. This assertion is well justified in the ray theory approximation and in view of the path integral formulation (3-26) for β .

A similar analysis which does not invoke the ray theory approximation leads to path integral corrections for both the amplitude *and phase*. Nevertheless, the corrections still take the form of integrals over the exact ray paths of the *lossless* Helmholtz equation. We will henceforth treat only the lossless Helmholtz equation since corrections for attenuation are easily computed and do not alter the exact ray paths (at least to first order).

E. REMARKS ON THE NATURE OF CLASSICAL RAY ACOUSTICS

It was shown in the preceding section that classical ray acoustics can provide only approximate solutions to the Helmholtz equation. The nature of the approximation is explored further in this section, where it is shown that classical ray acoustics is the high frequency limit of a nonuniform asymptotic expansion in which the ray paths are independent of frequency. Classical ray acoustics can also provide *exact* solutions to an important class of problems related to propagating discontinuities in the acoustic field.

1. Propagating discontinuities in the acoustic field

Consider an inhomogeneous quiescent medium which is suddenly disturbed by activating a point source, not necessarily time harmonic. We ask how much time must elapse before the disturbance can reach a distant observation point. Since the rate of propagation of the disturbance at any point in the medium is equal to the local speed of sound (or else what does "sound speed" mean for small signals in a medium at rest?), then the minimum travel time t_{\min} must be given by the path integral

$$\begin{aligned}
 t_{\min} &= \int \frac{ds}{c} \\
 &= \int \frac{(dx^2 + dy^2 + dz^2)^{1/2}}{c(x, y, z)} \\
 &= \int \frac{[(dx/ds)^2 + (dy/ds)^2 + (dz/ds)^2]^{1/2}}{c(x, y, z)} ds \\
 &= \int \frac{(x'^2 + y'^2 + z'^2)^{1/2}}{c(x, y, z)} ds \\
 &= \int \frac{(x'_i x'_i)^{1/2}}{c(x_i)} ds, \tag{3-27}
 \end{aligned}$$

where primes denote differentiation with respect to path length along a trajectory yet to be determined. Application of the variational calculus reveals that the path itself is the solution to [11,12]

$$\frac{d}{ds} \left(\frac{\partial F}{\partial x'_i} \right) - \frac{\partial F}{\partial x_i} = 0, \tag{3-28}$$

where

$$F = \frac{(x'_i x'_i)^{1/2}}{c(x_i)}. \tag{3-29}$$

Upon substituting Eq. (3-29) for F in Eq. (3-28) and using the auxiliary condition $x'_i x'_i = 1$, the path turns out to satisfy the *classical* ray path equation

$$\frac{d}{ds} \left(\frac{1}{c} \frac{d\mathbf{r}}{ds} \right) = \nabla \left(\frac{1}{c} \right).$$

In other words, no disturbance can reach the observation point due to the activity of the source before a minimum amount of time t_{\min} has elapsed, where t_{\min} is given by the classical ray path integral (3-27).⁵

⁵Nevertheless, propagation times apparently indicative of supersonic transmission speeds do occur occasionally even in linear theory, particularly during attempts to construct synthetic time series by Fourier synthesis of solutions to the lossy Helmholtz equation. The problem usually is due either

The preceding argument, though inspired by Fermat's principle and Hamilton's principle of least action, makes no reference to physical processes (in particular, the wave equation was never invoked); hence, it gives no assurance that any acoustical energy will actually flow along the classical ray paths and arrive at the times predicted by ray theory. Nevertheless, it does serve to establish a lower bound on transmission times. But there is a considerable body of literature, going back at least to Christoffel[15] in 1877, which shows that a surface across which the time derivatives of the acoustic field are discontinuous propagates according to the classical eikonal equation. Luneburg[16] obtained a similar result for electromagnetic propagation. Heller[17] obtained a generalized eikonal which allows for movement of the fluid medium. And Keller[18] showed that the transport equation governs the amplitudes of propagating discontinuities. The conclusion to be drawn from this is that classical ray theory is essentially a broadband theory best suited to the analysis of propagating fronts generated by pulsive sources.

2. Ray theory as a high frequency approximation

We seek an asymptotic solution of the Helmholtz equation for high frequencies by expanding in the small quantity $1/\omega$. Referring to the Sommerfeld representation of the acoustic field, $\Psi = Ae^{i\Phi}$, we express the exact eikonal as

$$\Phi = \omega\tau(\mathbf{r}), \quad (3-30)$$

while the amplitude is written as an asymptotic series:

$$A \sim \sum_{n=0}^{\infty} \left(\frac{i}{\omega}\right)^n A_n. \quad (3-31)$$

Note that τ , which will determine the ray trajectories, is independent of frequency. After substituting for Ψ in the Helmholtz equation, which is written in the form

$$\frac{1}{\omega^2} \nabla^2 \Psi + \frac{1}{c^2} \Psi = 0,$$

one obtains

$$e^{i\omega\tau} \sum_{n=0}^{\infty} \left(\frac{i}{\omega}\right)^n \left[A_n \left(\frac{1}{c^2} - \nabla\tau \cdot \nabla\tau \right) + \frac{i}{\omega} \left(2\nabla A_n \cdot \nabla\tau + A_n \nabla^2 \tau \right) + \frac{1}{\omega^2} \nabla^2 A_n \right] = 0. \quad (3-32)$$

cal analog of the Kramers-Kronig relations,[13,14] or to a failure of a saddle point approximation or other approximation method used to estimate group velocities. Either condition can result in predictions of spurious precursors to the earliest arrival predicted by ray theory. Fortunately, the intensities predicted for these premature arrivals are usually low enough that they can be tolerated without requiring corrective measures. Sometimes these acausal precursors are erroneously accepted at face value and attributed to mysterious "diffracted energy paths."

Since Eq. (3-32) is an identity in $1/\omega$, the coefficients of each power of $1/\omega$ must vanish independently. At lowest order in $1/\omega$ we recover the eikonal equation

$$\nabla\tau \cdot \nabla\tau = \frac{1}{c^2},$$

while the first order equation turns out to be the transport equation

$$2\nabla A_0 \cdot \nabla\tau + A_0 \nabla^2\tau = 0.$$

Thus classical ray acoustics is established as the asymptotic solution to the Helmholtz equation in the high frequency limit.

The remaining terms in Eq. (3-32) can be consolidated in like powers of $1/\omega$ and written in the form

$$\sum_{n=0}^{\infty} \left(\frac{i}{\omega}\right)^{n+2} \left(2\nabla A_{n+1} \cdot \nabla\tau + A_{n+1} \nabla^2\tau - \nabla^2 A_n\right) = 0,$$

which establishes the recursion relation

$$2\nabla A_{n+1} \cdot \nabla\tau + A_{n+1} \nabla^2\tau = \nabla^2 A_n \quad (3-33)$$

for the higher order terms in the asymptotic expansion. Note, though, that these terms affect only the amplitude A and not the ray paths, which are independent of frequency. The infinitesimal ray tube cross sections are not prevented from vanishing at caustics; hence, this perturbative treatment continues to predict nonphysical singular acoustic fields at caustics to any order in the expansion. The expansion is thus seen to be nonuniform when caustics are present.

Equation (3-33) would seem to offer a means of obtaining improved ray theory calculations by iteration, at least in regions free of caustics. The ray paths and the surfaces of constant phase form an orthogonal coordinate system. Pitre[19] points out that Eq. (3-33) can be rendered as an inhomogeneous transport equation in ray coordinates, and then converted into a ray path integral to be evaluated numerically. Chen and Ludwig[20] exploited this procedure to evaluate the importance of ray theory corrections.

However, the iterative correction scheme has liabilities as a practical computational procedure. The use of ray coordinates is not the problem; ray theory computer models which compute the rate of geometrical ray path spreading already have the information necessary to compute the Jacobian of the transformation from, say, cylindrical coordinates to ray coordinates. But $\nabla^2 A_n$ is not readily available and, in any case, the corrections are of dubious value even when they can be generated. The corrections are negligible far from caustics at the frequencies of interest in long range propagation. But if caustics are present then the corrections permit one to approach the caustic only a little more closely before the ray approximation fails; no amount of iteration will remove the singularity at the caustic or substantially improve the calculations near it. A glance ahead at the propagation loss curves of Fig. 4.5 on

page 37 will make this point clearer. Figure 4.5 is a comparison of the propagation loss computed using ray theory and also using Ludwig's uniform asymptotic formula, which is valid on and near the caustic. The ray theory propagation loss curves are indistinguishable from the uniform asymptotic propagation loss curves right up to the caustic, where ray theory becomes singular. The ray theory corrections offered by Eq. (3-33) are unnecessary far from the caustic and of little use near it.

IV. ILLUSTRATIVE APPLICATIONS OF EXACT RAY THEORY

Several derivations of classical ray theory were presented in the preceding chapter, and it was hinted that if the ray theory approximation were avoided then the resulting rays would be quite different. This chapter begins with the development of a simple computational procedure for numerically constructing exact ray diagrams whenever a solution to the Helmholtz equation is available. The remainder of the chapter is given over to demonstrations of the method.

A. A COMPUTATIONAL PROCEDURE FOR TRACING EXACT RAYS

Whenever a solution to the Helmholtz equation is known, it is possible to determine what the ray path trajectories *would* be if the ray theory approximation is not invoked. To see how this comes about, let us suppose that a solution Ψ to the Helmholtz equation is known for some particular source configuration and wave number $k(\mathbf{r})$ in a lossless medium. After computing the gradient of the defining equation for A and Φ , namely $\Psi = Ae^{i\Phi}$, one obtains

$$\frac{\nabla\Psi}{\Psi} = \frac{\nabla A}{A} + i\mathbf{K}.$$

Since A and $\mathbf{K} = \nabla\Phi$ are real, evidently

$$\frac{\nabla A}{A} = \text{Re} \left(\frac{\nabla\Psi}{\Psi} \right),$$

and

$$K \frac{d\mathbf{r}}{ds} = \text{Im} \left(\frac{\nabla\Psi}{\Psi} \right). \quad (4-1)$$

The latter is a first order differential equation for the ray path. It is desirable for computational reasons to eliminate K from the ray path equation by defining a new path parameter σ such that $K d\sigma = ds$. Then Eq. (4-1) becomes

$$\frac{d\mathbf{r}}{d\sigma} = \text{Im} \left(\frac{\nabla\Psi}{\Psi} \right). \quad (4-2)$$

One traces a ray by integrating Eq. (4-2), usually by numerical methods.

The equivalence of the first order ray path equation (4-1) and the second order equation (3-16) can easily be verified by substituting $Ae^{i\Phi}$ for Ψ in Eq. (4-1). One recovers the defining equation for the ray path tangent vector, $K d\mathbf{r}/ds = \nabla\Phi$, from which Eq. (3-16) was derived.

One can also calculate K by

$$K = \left| \text{Im} \left(\frac{\nabla\Psi}{\Psi} \right) \right|, \quad (4-3)$$

which result is achieved by computing $\mathbf{K} \cdot \mathbf{K}$ using Eq. (4-1). Also available is the amplitude A , by way of $A^2 = \Psi \Psi^*$.

That the ray path equation (4-2) is a first order differential equation has several remarkable consequences, two having to do with the computational process of solving ray path equations, or tracing rays, and another having to do with the qualitative behavior of the paths themselves. Only one initial condition is required in order to solve a first order differential equation, while a second order equation requires two initial or boundary conditions for its solution. To trace a classical ray one must solve the second order ray equation (3-18), which usually means that the ray trace must begin at the source (although the source need not be a point; it may be a surface), because only at the source are both the initial position *and direction* of the ray known. By contrast, given *any* starting point, the starting direction of an exact ray at that point is given by Eq. (4-2) because it is first order. Hence, an exact ray trace may commence anywhere.

Another useful consequence of the exact ray equation being first order is that eigenrays for arbitrary points can often be found by tracing the ray *backwards* from an observation point to the source. This is accomplished by requiring the numerical integrator to solve Eq. (4-2) for decreasing, rather than increasing, values of σ . The resulting ray trace will proceed from the observation point right back to the source.

The above should not be construed to mean that exact ray theory is a computational tool superior to classical ray theory. On the contrary, classical ray theory can generate approximate solutions to the Helmholtz equation *ab initio*, whereas exact ray tracing requires that a solution already be known. Nevertheless, the facility with which exact rays can be traced forwards or backwards from any starting position makes exact ray theory a versatile and illuminating alternative means of displaying and analyzing the acoustic field.

As promised earlier, we can also glean an insight into the qualitative behavior of exact rays from the fact that the ray path equation is first order. Since the particle velocity is a measurable quantity and must therefore be single valued at any position \mathbf{r} , and since the velocity potential satisfies the acoustic Helmholtz equation, it follows that the velocity potential is single valued and twice differentiable. Hence, the right hand side of Eq. (4-2) is single valued at \mathbf{r} . But this self-evident and seemingly innocuous observation means that the vector $d\mathbf{r}/d\sigma$ tangent to the ray path is unique, which in turn forces us to conclude that *only one ray passes through each point* \mathbf{r} . There is exactly one eigenray from a source to an observation point. The uniqueness of exact eigenrays stands in stark contrast to classical rays, which characteristically exhibit multipathing. This is an important realization and a source of considerable confusion; we will return to it several times.

The remainder of this chapter is devoted to demonstrations of exact ray analysis. Each case selected for analysis was chosen quite frankly for its pedagogical value by the following criteria: (1) Each case should serve as a canonical example of some problem frequently encountered in acoustics. For example, the Kormilitsin problem has as its dominant feature a smooth, convex caustic. The "harmonic oscillator"

waveguide was selected as a model of propagation in a duct. The circular piston is famous for its diffraction patterns, and so on. (2) Cases with published solutions are preferred, so that many readers will already be familiar with the problem. The intent is to maintain the focus on the exact ray theory developed here, and demonstrations of the theory are much more comprehensible when applied to familiar problems. (3) Each case has an exact analytic solution or a good approximate solution suitable for computation. Numerical solutions of the Helmholtz equation are avoided. This gives assurance that any unexpected behavior of the rays is in fact valid and cannot be attributed to the vagaries of numerical computation. To be sure, a Runge-Kutta-Fehlberg[21] numerical integration code is used to integrate the ray path equation, but many years of experience with numerical ray tracing have proven this procedure to be very reliable.[22] -[24] Acoustic propagation in realistic ocean environments is an extremely complicated process; sophisticated numerical computer models often must be used to obtain reasonably accurate simulations. To bring such models into play in all their complexity, while simultaneously trying to establish the fundamental properties of exact ray theory, would be an intolerable distraction for the purposes of this dissertation. Instead, we treat only cases where the acoustic field has reasonably simple behavior. This does not mean, however, that exact ray analysis is limited to "pencil and paper" problems. Some numerical propagation models can be modified to compute the acoustic field gradients as well as the field itself and to save them for use by a ray trace program. Such models would then be able to predict not only the *amplitude of the acoustic field but also its direction of propagation.*

There are two stages to the construction of the exact ray diagrams which follow. First, the Helmholtz equation is solved and the gradients of the acoustic field are computed, all by analytical methods. Then the ray path equation $dr/d\sigma = \text{Im } \nabla \Psi / \Psi$ is solved, usually by numerical integration. Since the solution to the Helmholtz equation is different for each case and usually rather complicated, the reader will find that somewhat lengthy and perhaps tedious mathematical preliminaries precede the generation of each ray diagram. I have tried to minimize the distraction of these mathematical excursions by simply providing a reference if a suitable solution has been published. There would be little point in reproducing solutions to problems selected in part because their solutions appear in the literature. Otherwise, I have tried to provide sufficient details of the development to allow reconstruction of the result without belaboring the derivation. For the most part, this material can be skimmed with little loss of continuity or comprehension.

B. THE UNBOUNDED HOMOGENEOUS MEDIUM CASE

As a simple demonstration of exact ray theory analysis we confirm that the exact ray trajectories are straight lines for the case of a point source in an unbounded homogeneous medium (the classical ray paths are also straight lines, of course).

The solution to the Helmholtz equation for a point source is

$$\Psi = Qe^{ikr}/r,$$

where Q is the source strength, with dimensions of volume per unit time, and r is the radial distance from the source, which is assumed to lie at the origin. Upon taking the gradient of Ψ and using $\nabla r = \mathbf{r}/r$, we find that

$$\frac{\nabla \Psi}{\Psi} = \left(ik - \frac{1}{r} \right) \frac{\mathbf{r}}{r}.$$

The ray paths are solutions to Eq. (4-1):

$$\begin{aligned} K \frac{d\mathbf{r}}{ds} &= \text{Im} \left(\frac{\nabla \Psi}{\Psi} \right) \\ &= k \frac{\mathbf{r}}{r}. \end{aligned}$$

But $K = k$ by Eq. (4-3), so the ray path equation is

$$\frac{d\mathbf{r}}{ds} = \frac{\mathbf{r}}{r}.$$

In words, the ray path tangent vector is the unit radial vector and the rays are therefore radial lines.

C. THE LINEAR SOUND SPEED CASE

Classical ray theory provides an exact solution to the Helmholtz equation when the sound speed is a constant. We now examine the linear sound speed profile case $c = az$, where classical ray theory, with a slight modification, still yields an exact solution. Most textbooks on underwater acoustics show that the rays for a linear profile are circular arcs centered on the surface,[2,7,10] as shown in Fig. 4.1.

Classical ray analysis of this problem produces the approximate solution

$$\begin{aligned} A &= \frac{2(z z_0)^{1/2}}{R_1 R_2}, \\ \Phi_{\text{ray}} &= 2 \frac{\omega}{a} \tanh^{-1} \left(\frac{R_1}{R_2} \right), \end{aligned} \quad (4-4)$$

for the acoustic field $\Psi = Ae^{i\Phi}$, where z_0 is the source depth and

$$R_1^2 = r^2 + (z - z_0)^2, \quad R_2^2 = r^2 + (z + z_0)^2.$$

Pekeris[25] showed that the exact solution results from modifying the phase (4-4) to

$$\Phi_{\text{exact}} = 2 \frac{\omega}{\alpha} \tanh^{-1} \left(\frac{R_1}{R_2} \right), \quad (4-5)$$

where

$$\alpha = \frac{a}{(1 - a^2/4\omega^2)^{1/2}}.$$

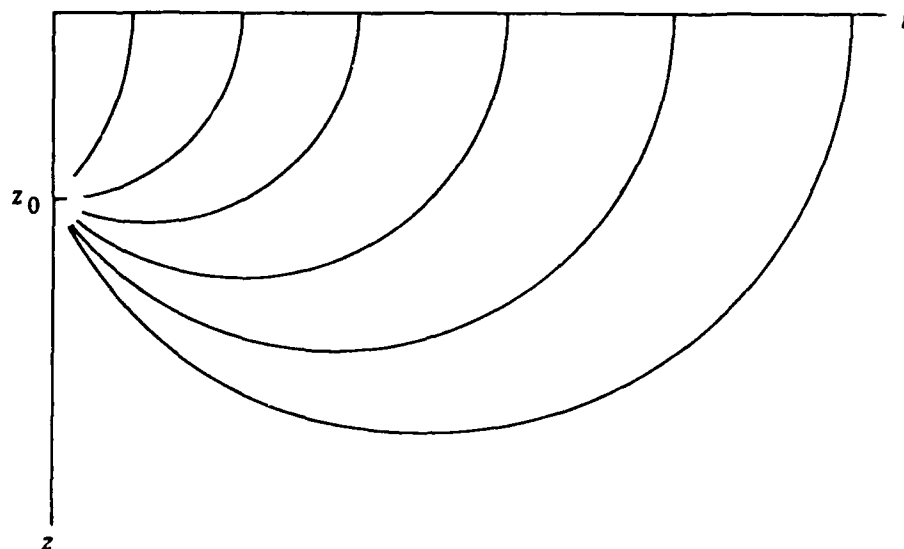


FIGURE 4.1 RAY PATHS FOR THE LINEAR SOUND SPEED PROFILE $c = az$. THIS UPWARDLY REFRACTING PROFILE IS NOTED FOR ITS CIRCULAR RAY ARCS.

The classical rays satisfy the first order path equation

$$\begin{aligned} \frac{d\mathbf{r}}{d\sigma} &= \nabla \Phi_{\text{ray}} \\ &= \frac{2\omega(R_2 \nabla R_1 - R_1 \nabla R_2)}{a(R_2^2 - R_1^2)}. \end{aligned}$$

Its solutions are the circular arcs noted earlier. But the exact rays satisfy

$$\begin{aligned} \frac{d\mathbf{r}}{d\sigma} &= \nabla \Phi_{\text{exact}} \\ &= \frac{2\omega(R_2 \nabla R_1 - R_1 \nabla R_2)}{\alpha(R_2^2 - R_1^2)}, \end{aligned}$$

which has the same circular arcs as its solutions. The exact rays, and the amplitudes associated with them, are exactly the same as their classical counterparts. However, the phase of an exact ray lags that of the classical ray.

D. A SMOOTH CAUSTIC SYSTEM

Exact ray analysis of the two preceding cases produced results which were little different from, or not at all different from, the classical ray theory results. If this always occurred then exact ray theory would be, at most, a perturbative correction to classical ray theory. We now treat a more typical problem, henceforth called the Kormilitsin problem after the original investigator, where the classical and exact ray diagrams are very different. The case $k^2 = k_0^2 z/z_0$, depicted in Fig. 4.2 along with the corresponding sound speed profile, is notable in that the classical ray diagram

exhibits a single smooth convex caustic and so serves as a canonical problem in the analysis of the field near a caustic.

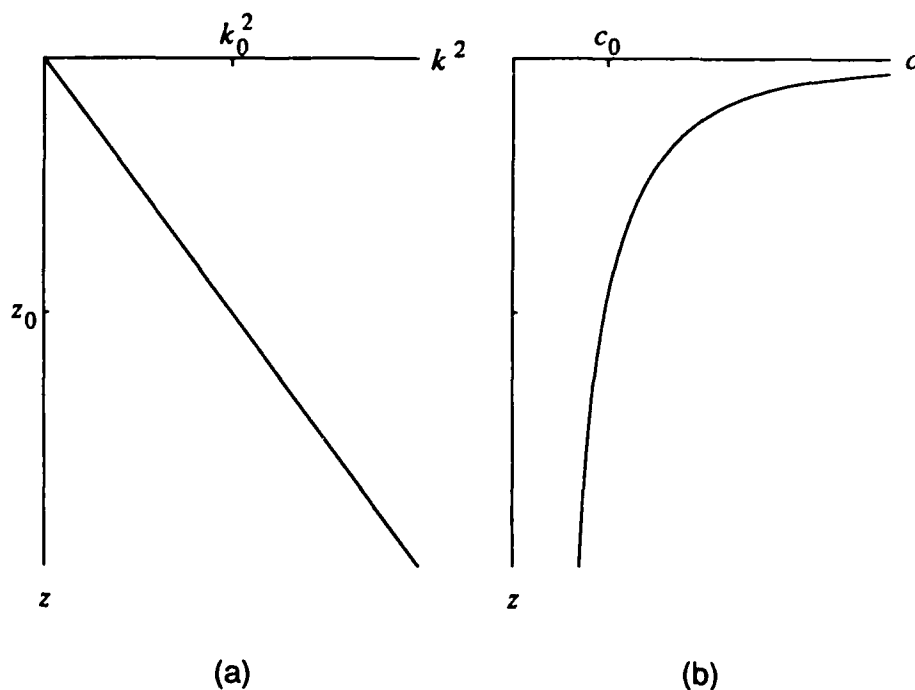


FIGURE 4.2 THE KORMILITSIN PROFILE. THE MONOTONIC DECREASE IN SOUND SPEED WITH DEPTH CAUSES DOWNWARD REFRACTION OF BOTH CLASSICAL AND EXACT RAY PATHS. (a) $k^2 = k_0^2(z/z_0)^{1/2}$. (b) $c = c_0(z_0/z)^{1/2}$.

Kormilitsin[26] obtained an exact elementary solution to the Helmholtz equation for a line source at z_0 ; the corresponding solution for a point source is[27]

$$\Psi = \left(\frac{k_0}{2\pi i} \right)^{1/2} \int_0^\infty \exp \left[ik_0 \left(\frac{1}{2\zeta} (r^2 + (z - z_0)^2) + \frac{\zeta}{4} (z + z_0) - \frac{\zeta^3}{96} \right) \right] \frac{d\zeta}{\zeta^{3/2}},$$

where $k_0 = k(z_0)$. Yet, for our purposes, a good approximation which lends itself readily to computation is preferable to a computationally resistant exact solution. Ludwig[28] and Kravtsov[29] independently developed a uniform asymptotic approximation specifically to compute the field near a simple caustic; it is therefore the method of choice for this problem. In deference to the fact that the uniform asymptotic expansion is an approximation, the rays generated from it will be referred to as frequency dependent rays rather than exact rays.

The development of several wave theoretical corrections to ray theory was motivated by a desire to retain the conceptual and computational advantages of ray theory while obtaining improved or corrected predictions where the ray theory approximation fails. Ludwig's uniform asymptotic approximation is an example of such a correction formula. Beam displacements, discussed in Sec. IV.H, are another.

These correction formulas typically make explicit use of classical eigenray path information already computed by ray models. Ludwig's formula makes use of classical ray amplitudes and phases and is easier to understand and interpret if the ray analysis is already completed. The introduction of Ludwig's formula is therefore postponed until after the classical ray analysis of the Kormilitsin profile problem which follows.

1. Classical ray analysis of the Kormilitsin profile

The classical ray analysis of the Kormilitsin profile begins with the determination of the ray trajectories. Once the ray paths are known the ray theoretical acoustic field amplitude and phase along a ray are readily found. It then remains to determine the rays which connect source and observation point; these are the eigenrays.

a. Ray trajectories

We obtain the classical ray paths in a range invariant medium by converting Snell's law,

$$k^2 \cos^2 \theta = k_0^2 \cos^2 \theta_0,$$

into a differential equation whose solution reduces to quadrature. Here, θ is the ray path angle measured with respect to the horizontal. Snell's law is rendered as

$$\cot \theta = \frac{k_0 \cos \theta_0}{(k^2(z) - k_0^2 \cos^2 \theta_0)^{1/2}} \quad (4-6)$$

with the aid of trigonometric identities. Since θ is the ray path angle (θ_0 is the path angle at the source, or "launch angle"), the derivative of the ray path range with respect to depth is given by $dr/dz = \cot \theta$. Equation (4-6) may therefore be regarded as a first order differential equation. Moreover, the right hand side of Eq. (4-6) is a function of z only; hence Eq. (4-6) may be integrated at once to yield

$$r = \int_{z_0}^z \frac{k_0 \cos \theta_0}{(k^2(z') - k_0^2 \cos^2 \theta_0)^{1/2}} dz'. \quad (4-7)$$

Setting $k^2 = az$ in Eq. (4-7) and integrating, we find

$$r = 2z_0^{1/2}(z^{1/2} \sin \theta - z_0^{1/2} \sin \theta_0) \cos \theta_0.$$

Inverted, this is

$$z = z_0 + r \tan \theta_0 + r^2 / (4z_0 \cos^2 \theta_0). \quad (4-8)$$

Thus the ray paths shown in Fig. 4.3 are parabolic arcs.

b. Amplitude

For a point source on the z axis in a range invariant medium, the classical ray amplitude is obtained from

$$A^2 = 1/r|\zeta|, \quad (4-9)$$

where ζ is the derivative of the ray path depth with respect to launch angle at constant range. For the Kormilitsin profile this is

$$\begin{aligned} \zeta &= \left. \frac{\partial z}{\partial \theta_0} \right|_r \\ &= r \sec^2 \theta_0 \left(1 + \frac{r}{2z_0} \tan \theta_0 \right). \end{aligned} \quad (4-10)$$

From Eq. (4-10) and the ray path equation (4-8), the surface $\zeta = 0$ is found to be

$$r_c^2 = 4z_0z_c.$$

The locus of points (r_c, z_c) defines a parabolic surface which forms an envelope to the rays and separates the region containing rays (the insonified region) from the region devoid of rays (the shadow zone), as shown in Fig. 4.3. Such surfaces are called caustics because of the unusually intense acoustic fields which develop along them at high frequencies. The classical ray amplitude is singular on a caustic.

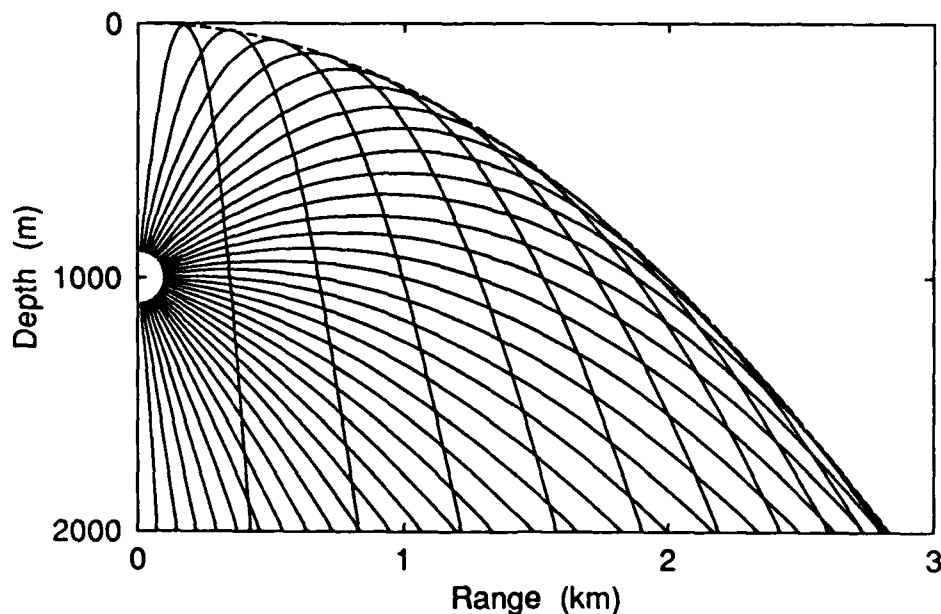


FIGURE 4.3 CLASSICAL RAY DIAGRAM FOR THE KORMILITSIN PROFILE. THE PARABOLIC RAY PATHS (SOLID CURVES) ALL EVENTUALLY GRAZE THE CAUSTIC (DASHED CURVE), WHICH IS ALSO PARABOLIC.

c. Phase

The phase in the ray theory approximation is given by the path integral

$$\Phi = \int_0^s k ds',$$

or

$$\Phi = \int_0^r k[1 + (dz/dr')^2]^{1/2} dr'$$

in cylindrical coordinates. Using $k^2 = az$ and Eq. (4-6), the phase integral becomes

$$\Phi = \left(\frac{a}{z_0}\right)^{1/2} \sec \theta_0 \int_0^r z(r') dr'.$$

Integration of the ray path equation (4-8) then gives

$$\Phi = k_0 r \sec \theta_0 \left[1 + \frac{r}{2z_0} \tan \theta_0 + \frac{1}{3} \left(\frac{r}{2z_0}\right)^2 \sec^2 \theta_0 \right]. \quad (4-11)$$

d. Eigenrays

Since $\sec^2 \theta_0 = 1 + \tan^2 \theta_0$, Eq. (4-8) is seen to be quadratic in $\tan \theta_0$ as well as r . The two roots of Eq. (4-8) for a point (r, z) yield the launch angles of the two eigenrays, or rays which connect the source at (r_0, z_0) to the point (r, z) :

$$\tan \theta_0^\pm = \frac{2z_0}{r} \left[\pm \left(\frac{z}{z_0} - \frac{r^2}{4z_0^2} \right)^{1/2} - 1 \right]. \quad (4-12)$$

The eigenray launched at θ_0^- grazes the caustic before reaching the observation point, while the eigenray launched at θ_0^+ passes through the observation point before grazing the caustic. Henceforth, all ray path parameters pertaining to the eigenray which grazes the caustic before reaching the observation point will bear the superscript 1, while path parameters of the second eigenray will carry the subscript 2.

Thus the acoustic field in the insonified region is given in the ray theory approximation by the coherent sum of the pressure contributions of the two eigenrays:

$$\Psi_{\text{ray}} = A_1 e^{i\Phi_1} + A_2 e^{i\Phi_2},$$

where the amplitudes A_2^1 are given by Eqs. (4-9) and (4-10) and the phases Φ_2^1 are given by Eq. (4-11). The launch angles of the eigenrays are obtained from Eq. (4-12).

2. Ludwig's uniform asymptotic approximation

Having obtained the classical ray theoretical solution to the Kormilitsin problem, we are now prepared to introduce Ludwig's formula. At lowest order in $1/\omega$, Ludwig's approximate solution to the Helmholtz equation is

$$\Psi = 2\pi^{1/2} e^{-i\pi/4} e^{i\Theta(r)} [g^+(r) \text{Ai}(-\xi(r)) + ig^-(r) \text{Ai}'(-\xi(r))], \quad (4-13)$$

where

$$\xi = \left[\frac{3}{4}(\Phi^1 - \Phi_2) \right]^{2/3}, \quad \Theta = \frac{1}{2}(\Phi^1 + \Phi_2), \quad g^\pm = \frac{1}{2}\xi^{\pm 1/4}(A^1 \pm A_2). \quad (4-14)$$

Notice the use of the classical eigenray amplitudes and phases in Eqs. (4-14).

The Airy function Ai is a solution to Airy's differential equation[30]

$$\text{Ai}''(x) = x \text{Ai}(x).$$

It is oscillatory for $x < 0$ and decays exponentially for $x > 0$.

The gradient of the acoustic field is needed in order to trace frequency dependent rays. After calculating the gradients of Eqs. (4-13) and (4-14), we get

$$\frac{\nabla \Psi}{\Psi} = \frac{\text{Ai}(-\xi)\Gamma_1 + \text{Ai}'(-\xi)\Gamma_2}{g^+ \text{Ai}(-\xi) + ig^- \text{Ai}'(-\xi)}, \quad (4-15)$$

where

$$\begin{aligned} \Gamma_1 &= ig^+ \nabla \Theta + \nabla g^+ + i\xi g^- \nabla \xi, \\ \Gamma_2 &= -g^- \nabla \Theta + i \nabla g^- - g^+ \nabla \xi, \end{aligned}$$

and

$$\begin{aligned} \nabla \xi &= \frac{1}{2}\xi^{-1/2}(\nabla \Phi^1 - \nabla \Phi_2), \\ \nabla \Theta &= \frac{1}{2}(\nabla \Phi^1 + \nabla \Phi_2), \\ \nabla g^\pm &= \pm \frac{1}{4}g^\pm \frac{\nabla \xi}{\xi} + \frac{1}{2}\xi^{\pm 1/4}(\nabla A^1 \pm \nabla A_2). \end{aligned} \quad (4-16)$$

Before computing the gradients of the classical ray quantities appearing in Eqs. (4-16), it proves convenient to define the following variables:

$$l = z/z_0, \quad m = r/2z_0, \quad n^2 = (1 + m \tan \theta_0)^2.$$

Then the ray path equation may be written compactly as

$$l = m^2 + n^2,$$

the eigenray amplitudes are

$$A_2^1 = \frac{1}{2z_0[n(1 + l \pm 2n)]^{1/2}},$$

and the phases are

$$\Phi_2^1 = \frac{2}{3}k_0 z_0(1 + l \mp n)(1 + l \pm 2n)^{1/2}.$$

The gradients of the eigenray amplitudes and phases appearing in Eq. (4-16) take the forms

$$\nabla A_2^1 = \frac{z_0}{n}(A_2^1)^3[\mathbf{e}_r m(1 + l \pm 4n) - \mathbf{e}_z(1 + l \pm 4n + 2n^2)] \quad (4-17)$$

and

$$\nabla \Phi_2^1 = \frac{k_0}{(1 + l \pm 2n)^{1/2}}[\mathbf{e}_r m + \mathbf{e}_z(l \pm n)]. \quad (4-18)$$

3. Frequency dependent ray analysis of a caustic

With Eqs. (4-15) - (4-18) in hand for $\nabla\Psi/\Psi$, a frequency dependent ray diagram is constructed by numerically solving the ray path equation $dr/d\sigma = \text{Im}(\nabla\Psi/\Psi)$ for various launch angles, using mathematical software library routines to compute A_i and A_i' . These routines must be capable of computing Airy functions of complex argument if the shadow zone is to be treated.

Figure 4.4 shows the frequency dependent ray diagrams for source frequencies of 5 Hz and 50 Hz, with the source located 1000 m below the surface and a sound speed at the source of 1500 m/s. These frequency dependent rays obviously differ starkly from their classical counterparts shown in Fig. 4.3. The frequency dependent ray diagrams can be divided roughly into four zones according to the behavior of the rays found within them. Near the source the rays form the radial lines characteristic of spherical spreading, as discussed in Sec. IV.B. In the insonified region far from the source but well inside the caustic, the frequency dependent rays begin to undulate. As the rays approach the caustic, the undulations damp out and the rays bunch together, running parallel to each other and almost parallel to the caustic. The greatest constriction of the ray bundles is found somewhat inside the caustic. Eventually, the rays cross the caustic and intrude into the shadow zone, where they begin to spread out. And, in sharp contrast to the classical rays, these rays never cross. In fact they fill all of space, so that for every observation point, even in the shadow zone, there is exactly one eigenray.

The details of these strange behaviors are sensitive to the source frequency. The amplitudes of the undulations diminish with increasing frequency, but the undulations become more rapid, giving the 50 Hz rays a "jittery" appearance. Even though they were launched at the same angles as the 5 Hz rays (from -85° to $+85^\circ$ in 5° increments), the 50 Hz rays are much more concentrated near the caustic and reach their greatest concentration nearer the caustic. Nor do they venture nearly as far out into the shadow zone as the 5 Hz rays.

The frequency dependent ray diagrams can be used to explain the behavior of propagation loss curves. Horizontal reference lines are drawn across both ray diagrams in Fig. 4.4 at the 1200 m depth level. Figure 4.5 shows the propagation loss curves at this depth for both frequencies, computed by Ludwig's uniform asymptotic approximation (solid curves) and by classical ray theory (dashed curves). (The propagation loss curves plotted here were computed using the formula $PL = -10 \log_{10}[\Psi\Psi^*]$.) The ray theory propagation loss curve is extended into the shadow zone by a slight modification of classical ray theory to be described later. The ray theory results agree very closely with the uniform asymptotic approximation except in the vicinity of the caustic.

The separation between the rays as they cross the reference line is a measure of the spreading of the rays and, hence, the intensity of the acoustic field. Comparing the 5 Hz ray diagram with the corresponding propagation loss curve, we see that wherever the undulations of a pair of rays causes them to draw apart as they cross

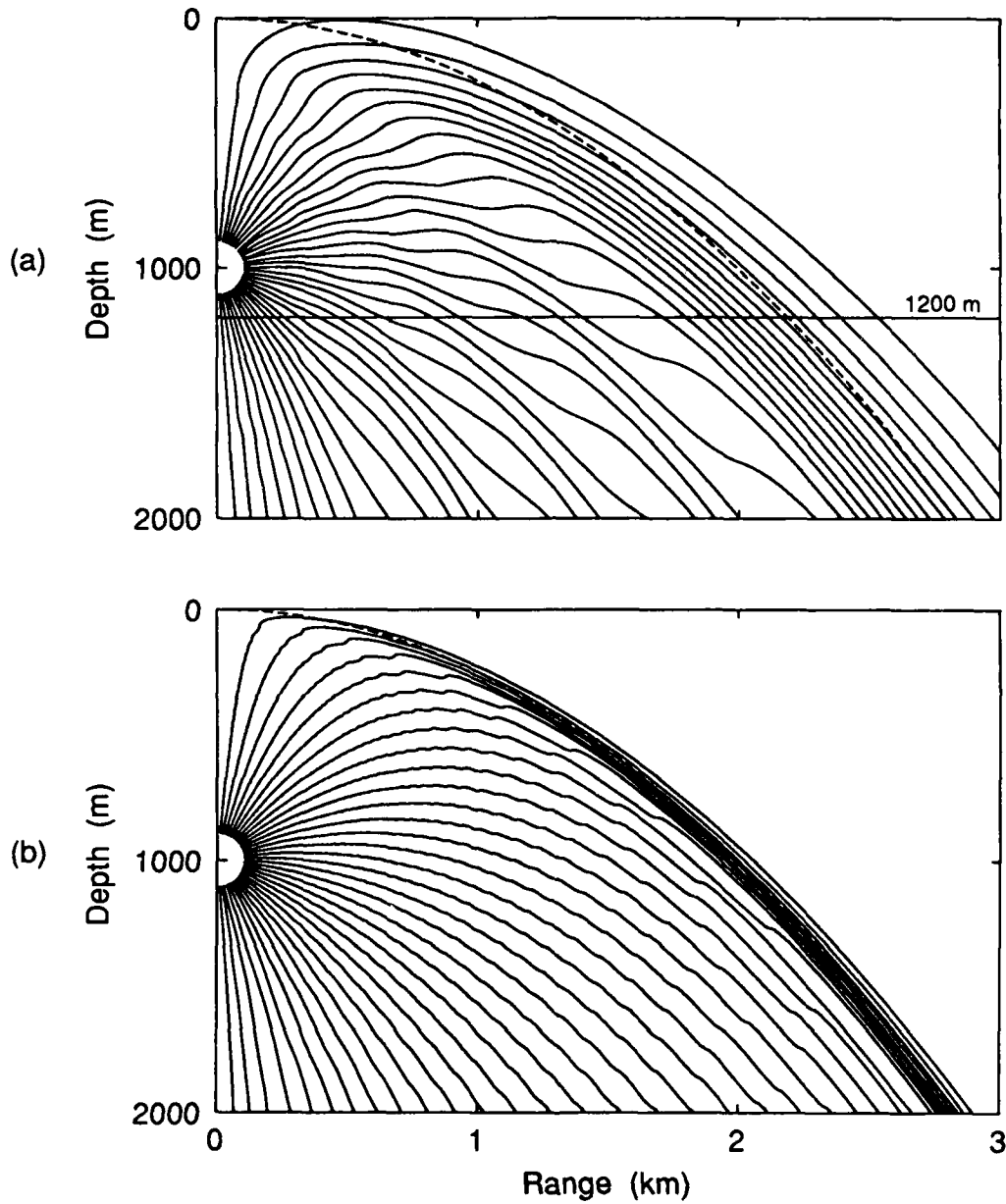


FIGURE 4.4 FREQUENCY DEPENDENT RAY DIAGRAM FOR THE KORMILITSIN PROFILE. (a) AT 5 Hz THE RAYS UNDULATE GENTLY AND READILY INTRUDE INTO THE SHADOW ZONE. (b) AT 50 Hz THE UNDULATIONS ARE MUCH MORE RAPID AND OF SMALLER AMPLITUDE. PENETRATION OF THE SHADOW ZONE IS GREATLY REDUCED.

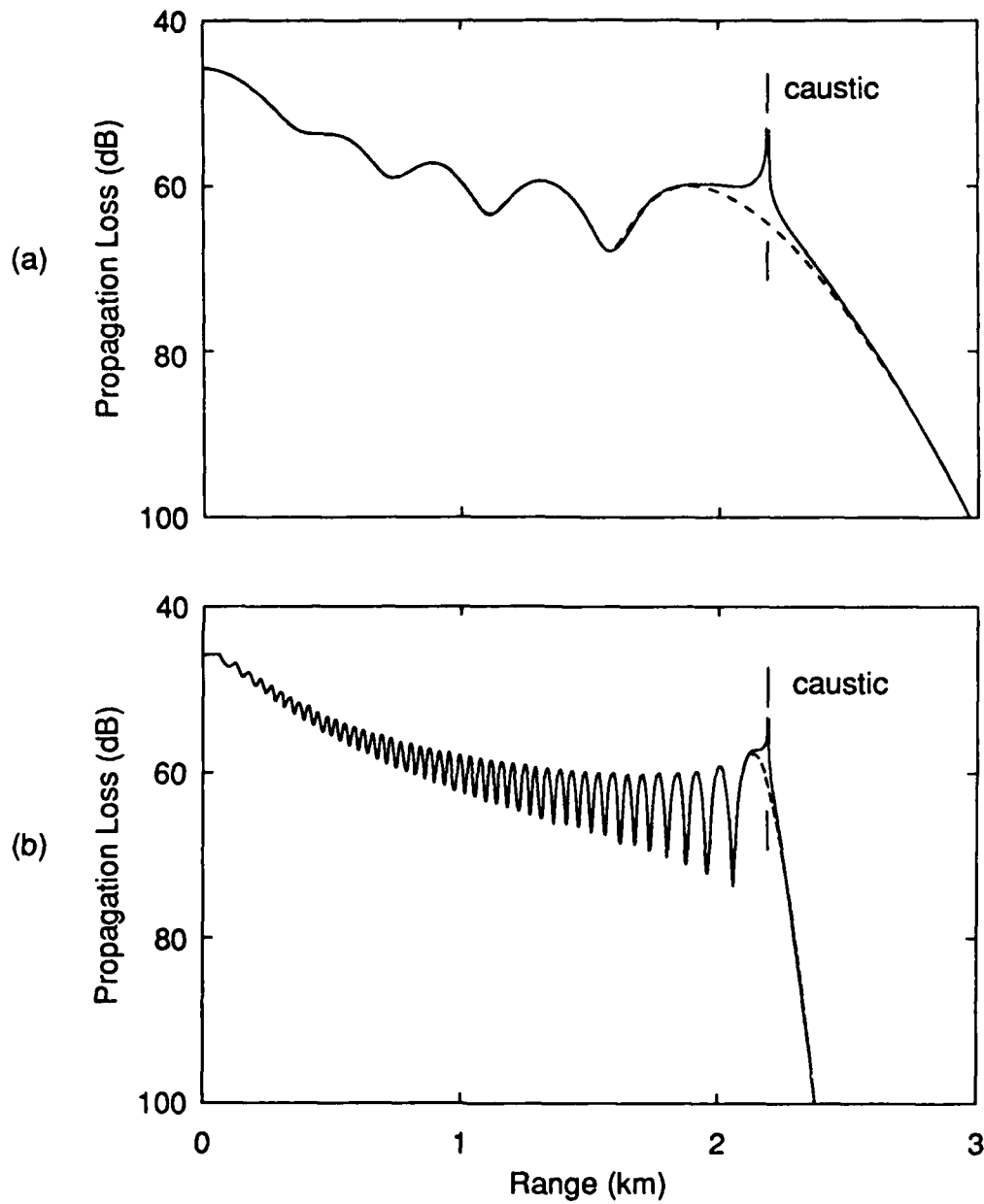


FIGURE 4.5 PROPAGATION LOSS CURVES FOR THE KORMILITSIN PROFILE. THE BROKEN VERTICAL LINE INDICATES THE RANGE OF THE CAUSTIC AT $z = 1200$ m. THE SOURCE IS AT 1000 m, OBSERVATION POINTS ARE AT 1200 m. (a) 5 Hz. (b) 50 Hz.

the reference line there is a dip in the field intensity over the corresponding range interval; similarly, the intensity is greatest where the ray pair draws together. The undulations vanish as the reference line nears the caustic; the rays become most concentrated just inside the caustic and then begin to spread out as the reference line passes through the caustic and into the shadow zone. Likewise, the intensity reaches its maximum at the point of maximum concentration of the rays and then decays monotonically as the range increases to and beyond the range of the caustic.

The 50 Hz ray diagrams and propagation loss curves possess the same general features as those for 5 Hz but differ in the details. The rapid undulations of the rays correspond to the rapid oscillations in the field intensity. The heavier concentration of rays nearer the caustic and the lesser degree of intrusion into the shadow zone coincides with the peak intensity occurring nearer the caustic and the rapid exponential decay of the field in the shadow zone.

The propagation loss curves are interesting in their own right and deserve a few remarks. Comparison of ray theory with uniform asymptotic predictions confirms the maxim that ray theory remains valid in the insonified region up to the last zone of constructive interference just inside the caustic. The acoustic field intensity reaches a local maximum in this zone and then begins to decay. The intensity on the caustic itself is actually several decibels below the local maximum.

But notice that the "classical" ray theory propagation loss curve continues into the shadow zone even though the classical ray diagram of Fig. 4.3 clearly shows the rays confined to the insonified region. This portion of the propagation loss curve was generated using the complex ray theory of White and Pedersen.[31] We had assumed until now that only real-valued eigenray launch angles and ray path coordinates are admissible. But the ray path equation (4-8) is quadratic in $\tan \theta_0$ and yields complex-valued eigenray launch angles for observation points in the shadow zone. The path parameters of rays with complex launch angles take on complex values. Ludwig's asymptotic formula (4-13) remains valid in the shadow zone and makes explicit use of the complex amplitudes and phases of the complex eigenrays. Following White and Pedersen, we compute the field in the shadow zone by retaining the complex eigenray labeled 2, but discard the eigenray labeled 1 because it gives rise to a nonphysical exponentially growing field. In other words $\Psi = A^1 e^{i\phi^1} + A_2 e^{i\phi^2}$ in the insonified region, but $\Psi = A_2 e^{i\phi^2}$ in the shadow zone.

E. REMARKS ON THE NATURE OF EXACT RAY THEORY

Unlike the first two cases examined in this chapter, the frequency dependent rays for the Kormilitzin profile are irreconcilably different from their classical counterparts; yet both kinds of rays are purported to represent the paths of energy propagation. It seems appropriate to try to resolve the paradox before proceeding to more demonstrations of exact ray theory.

The solution to the dilemma lies in the nature of classical ray theory and the ray theory approximation. Classical ray theory has been used for many decades to study wave propagation and researchers have thereby gained a great deal of expe-

rience and intuition which guides their expectations of the behavior of rays. It is therefore disconcerting to many people to be confronted with exact ray diagrams which systematically violate their expectations of what ray diagrams should look like. It is tempting to dismiss these curves as being something other than rays (and, to be sure, they are indeed not classical rays). But, although it is certainly correct to claim, for example, that these paths are the orthogonal trajectories of the solution to the Helmholtz equation, this assertion does not serve to distinguish these paths as something other than rays. These are precisely the paths which result from avoiding the approximation invoked in the Sommerfeld derivation of the classical ray path equation; they form, now with perfect fidelity, the energy flux tubes which are the essential feature of a ray theory. In short, these paths are rays.

Another tempting resolution of the paradox, also incorrect, is to suppose that if exact rays were constructed at high enough frequencies then they would come to resemble classical rays, because classical ray theory is a high frequency approximation. But this expectation will usually be frustrated, if for no other reason than because exact ray diagrams never exhibit multipathing no matter how high the source frequency, whereas multipathing is a characteristic feature of most classical ray diagrams. Classical ray theory is indeed a high frequency asymptotic approximation, but the asymptotic expansion is *nonuniform* in most cases, and the nonuniformity manifests in the vicinity of caustics. Caustics are an inevitable consequence of multipathing; if the ray paths cross at all then there will usually be a limiting surface where the rays cross tangentially. Such a surface is, of course, a caustic, and the differential ray tube cross sectional areas vanish on the caustic. The transport equation then predicts nonphysical singular acoustic fields on the caustic.

When the classical ray path equation is derived by the Sommerfeld development rather than as a high frequency approximation, one makes the ray theory assumption that $\nabla^2 A/A \ll k^2$. But this assumption usually turns out to be much more than a perturbative approximation; the invocation of the ray theory approximation changes the resulting rays from exact rays to classical rays which may behave quite differently.

Yet classical ray theory has been used to solve the Helmholtz equation for many years and with considerable success. If further proof were needed, the propagation loss curves computed for the Kormilitsin profile using classical ray theory agree extremely well with those computed by Ludwig's uniform asymptotic approximation, except near the caustic. Classical ray theory was clearly not "wrong" in that case, so why were the classical rays so uncompromisingly different from the frequency dependent rays? In particular, why is the phenomenon of multipathing, so familiar in classical ray diagrams, absent from exact ray diagrams?

In order to solve the multipathing conundrum, we revisit the Kormilitsin problem, but now we consider a quiescent medium disturbed by a point source which is suddenly activated. The reader will recall from the discussion in Sec. III.D.1 that the leading edge of the resulting disturbance propagates according to the predictions of classical ray theory. Specifically, a listener in the insonified region will note two distinct arrivals at times and intensities predicted by ray theory, the first arrival be-

ing from that portion of the surface formed by the propagating discontinuity which encountered the caustic before sweeping past the listener. The predictions of classical ray theory are also in accord with common experience of multipathing in the form of echoes. Ray theory is unsurpassed at tracking propagating discontinuities.

Multipathing, whether due to reflection or refraction, is a quintessentially broadband phenomenon. But a listener exposed to a continuous wave (cw) source hears only a pure tone; there is no sensation of distinct arrivals—no multipathing. Whereas classical ray theory describes the broadband phenomenology to which it is better suited, exact ray theory describes cw phenomenology, and the two are simply different.

One can reconstruct the acoustic disturbance created by a broadband source by Fourier synthesis of the acoustic fields generated by cw sources, each radiating at a different frequency. The acoustic fields of each cw source are best represented by exact rays, while the broadband disturbance is best represented by classical rays. When one applies classical ray theory to the Helmholtz equation, one presses into service the solution to a broadband problem in order to solve a cw problem. This is permissible—at the cost of failures of the theory near caustics, as is well understood. It is less well understood that classical ray theory comes freighted with the conceptual baggage of broadband propagation. Ironically, much of the conceptual framework and many intuitive notions of the behavior of cw fields are based on experience with classical ray theory.

F. PROPAGATION IN A WAVEGUIDE

Next we treat the case where $k^2(z)$ is taken to be the quadratic function

$$k^2 = k_a^2[1 - (1 - z/z_a)^2]. \quad (4-19)$$

Thus k has a maximum value of k_a at $z = z_a$, and vanishes at $z = 0$ and $z = 2z_a$, as shown in Fig. 4.6(a). Figure 4.6(b) shows that the corresponding sound speed profile $c(z) = \omega/k(z)$ has a minimum value of c_a at the axis depth z_a and increases without bound near the asymptotes at $z = 0$ and $z = 2z_a$. Sound tends to refract away from regions of high sound speed and toward regions of low speed. This medium therefore acts as a waveguide even though it lacks true boundaries, turning both classical and exact rays away from the asymptotes and steering the acoustic energy towards the sound channel axis. The waveguide thus formed turns out to be the acoustic analog of the quantum harmonic oscillator and henceforth will be called the harmonic oscillator waveguide.

1. Classical ray analysis of the harmonic oscillator waveguide

The classical ray paths may be determined, as in the case of the Kormilitsin problem, by integrating Snell's formula:

$$r = \int_{z_0}^z \frac{k_0 \cos \theta_0}{[k^2(z') - k_0^2 \cos^2 \theta_0]^{1/2}} dz'.$$

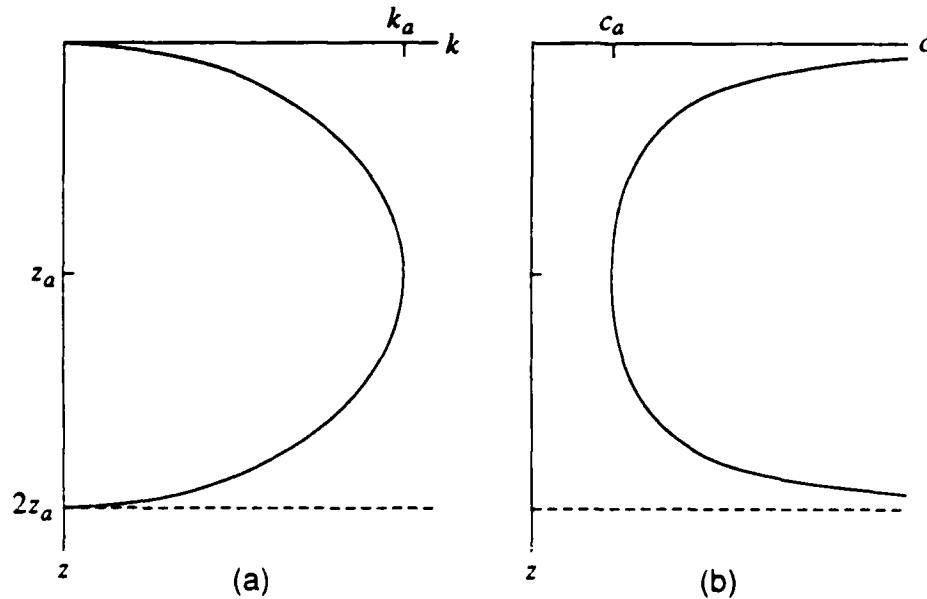


FIGURE 4.6 THE HARMONIC OSCILLATOR WAVEGUIDE. (a) $k^2 = k_a^2[1 - (1 - z/z_a)^2]$. (b) $c = c_a[1 - (1 - z/z_a)^2]^{1/2}$.

Quadrature is simplified when the source is located on the axis. Not surprisingly, in view of the nature of the waveguide, the ray paths turn out to be sinusoidal:

$$z = z_a + z_a \sin \theta_0 \sin \left(\frac{r}{z_a \cos \theta_0} \right).$$

The rate of change of ray path depth with respect to launch angle is

$$\begin{aligned} \zeta &= \left. \frac{\partial z}{\partial \theta_0} \right|_r \\ &= z_a \cos \theta_0 \sin \left(\frac{r}{z_a \cos \theta_0} \right) + r \tan^2 \theta_0 \cos \left(\frac{r}{z_a \cos \theta_0} \right). \end{aligned}$$

Caustics are located where $\zeta = 0$. For a given launch angle θ_0 , the ranges $r_c(\theta_0)$ at which the ray grazes the caustic turn out to satisfy the nonlinear equation

$$\frac{\tan(r_c/z_a \cos \theta_0)}{r_c/z_a \cos \theta_0} = -\tan^2 \theta_0.$$

while the corresponding depths $z_c(r_c, \theta_0)$ satisfy the ray path equation

$$z_c = z_a + z_a \sin \theta_0 \sin \left(\frac{r_c}{z_a \cos \theta_0} \right).$$

2. Normal mode representation of the field in a waveguide

Waveguide problems can often be solved conveniently using normal modes (a brief review of the method follows), although the normal modes and eigenvalues must

usually be determined numerically. The profile (4-19) selected for this example is one of very few problems in which the normal modes and eigenvalues can be expressed analytically and computed easily.

The Green function $\Psi_G(\mathbf{r}; \mathbf{r}_0)$ satisfies the inhomogeneous Helmholtz equation

$$\nabla^2 \Psi_G + k^2 \Psi_G = -\delta(\mathbf{r} - \mathbf{r}_0).$$

In cylindrical coordinates this is

$$\left[\frac{1}{r} \frac{\partial}{\partial r} \left(r \frac{\partial}{\partial r} \right) + \frac{\partial^2}{\partial z^2} + \frac{1}{r^2} \frac{\partial^2}{\partial \phi^2} \right] \Psi_G + k^2 \Psi_G = -\frac{1}{r} \delta(r - r_0) \delta(z - z_0) \delta(\phi - \phi_0). \quad (4-20)$$

Because the source is located on the z axis and the medium is horizontally stratified, the acoustic field is azimuthally symmetrical and derivatives with respect to ϕ consequently vanish. The inhomogeneous Helmholtz equation (4-20) becomes

$$\frac{\partial^2 \Psi_G}{\partial r^2} + \frac{1}{r} \frac{\partial \Psi_G}{\partial r} + \frac{\partial^2 \Psi_G}{\partial z^2} + k^2 \Psi_G = -\frac{1}{r} \delta(r - r_0) \delta(z - z_0) \delta(\phi). \quad (4-21)$$

Integration of Eq. (4-21) with respect to ϕ from 0 to 2π produces the desired form of the inhomogeneous Helmholtz equation:

$$\frac{\partial^2 \Psi_G}{\partial r^2} + \frac{1}{r} \frac{\partial \Psi_G}{\partial r} + \frac{\partial^2 \Psi_G}{\partial z^2} + k^2 \Psi_G = -\frac{1}{2\pi r} \delta(r) \delta(z - z_0). \quad (4-22)$$

Since the homogeneous Helmholtz equation corresponding to Eq. (4-22) is separable, it is convenient to express the solution to the inhomogeneous Helmholtz equation in terms of the solutions to the separated depth and radial equations. It can be shown that the Green function for Eq. (4-22) is given by (see Boyles,[2] pp. 163-177)

$$\Psi_G(r, z; z_0) = \frac{i}{4} \sum_{n=0}^{\infty} u_n(z_0) u_n(z) H_0^{(1)}(k_n r). \quad (4-23)$$

The radial function $H_0^{(1)}$, the function of the first kind, is a solution of a Bessel equation which may be written in the form

$$r^2 \frac{d^2}{dr^2} R_0(\kappa r) + r \frac{d}{dr} R_0(\kappa r) + \kappa^2 r^2 R_0(\kappa r) = 0.$$

$H_0^{(1)}(\kappa r)$ is that solution to the Bessel equation which is singular at $r = 0$ and which is consistent with outgoing waves and an acoustic field with time dependence $e^{-i\omega t}$; that is, it satisfies the Sommerfeld radiation condition

$$\lim_{r \rightarrow \infty} r^{1/2} \left(\frac{d H_0^{(1)}}{dr}(\kappa r) - i k_n H_0^{(1)}(\kappa r) \right) = 0.$$

The normal modes $u_n(z)$ are the eigenfunctions of the depth-separated Helmholtz equation

$$\frac{d^2 u_n}{dz^2} + (k^2 - k_n^2)u_n = 0, \quad (4-24)$$

and the k_n^2 are the corresponding eigenvalues. The normal modes satisfy the orthonormality condition

$$\int_{-\infty}^{\infty} u_m(z)u_n(z) dz = \delta_{mn},$$

and boundary or radiation conditions imposed on Ψ and $\partial\Psi/\partial z$ at horizontal boundary surfaces.

In the case of the harmonic oscillator waveguide, the normal modes are expressible in terms of Hermite polynomials[30]:

$$\begin{aligned} u_n(z) &= N_n e^{-x^2/2} H_n(x), \\ x &= k_a^{1/2} z_a^{-1/2} (z - z_a), \\ N_n &= k_a^{1/4} z_a^{-1/4} \pi^{-1/4} 2^{-n/2} (n!)^{-1/2}, \end{aligned}$$

and the eigenvalues are equally spaced in increments of $2k_a/z_a$:

$$k_n^2 = k_a^2 - (2n + 1)k_a/z_a. \quad (4-25)$$

The Hermite polynomials H_n (not to be confused with Hankel functions, such as $H_n^{(1)}$) satisfy the differential equation

$$H_n''(x) - 2xH_n'(x) + 2nH_n(x) = 0,$$

and the normalization condition

$$\int_{-\infty}^{\infty} e^{-x^2} [H_n(x)]^2 dx = 2^n \pi^{1/2} n!.$$

They are easily computed, along with their derivatives, using the recursion relations

$$\begin{aligned} H_n(x) &= 2xH_{n-1}(x) - 2(n-1)H_{n-2}(x), \\ H_0(x) &= 1, \\ H_1(x) &= 2x, \end{aligned}$$

and the differentiation formula

$$H_n'(x) = 2nH_{n-1}(x). \quad (4-26)$$

One of the properties of a waveguide is that not all modes propagate freely within it; beyond some mode cutoff number n_c the modes are damped exponentially as they travel down the waveguide. We exploit this property to terminate the normal mode summation (4-23). For the harmonic oscillator waveguide, mode cutoff occurs at

$$n_c = \lfloor \frac{1}{2}(k_a z_a - 1) \rfloor. \quad (4-27)$$

The eigenvalues are negative for modes with $n > n_c$, as one may confirm by inspection of the dispersion relation (4-25). The argument of the Hankel function, $k_n r$, is consequently imaginary for modes above cutoff. For large argument w , the Hankel function has the asymptotic form

$$H_0^{(1)}(w) \sim \sqrt{\frac{2}{\pi w}} e^{i(w-\pi/4)},$$

hence, for a purely imaginary argument $w = ix$,

$$H_0^{(1)}(ix) \sim -i \sqrt{\frac{2}{\pi x}} e^{-x}.$$

Modes above cutoff are thus exponentially damped and do not propagate very far down the waveguide. One may therefore truncate the mode summation at cutoff, provided the calculations are restricted to ranges beyond the effective propagation distance of the first damped mode.

We are not quite ready to trace rays; we still need $\nabla\Psi$. The gradient of the mode sum (4-23) for Ψ is

$$\begin{aligned} \nabla\Psi_G &= \frac{i}{4} \sum_0^{\infty} u_n(z_0) \nabla[u_n(z) H_0^{(1)}(k_n r)] \\ &= \frac{i}{4} \sum_0^{\infty} u_n(z_0) [e_z u_n'(z) H_0^{(1)}(k_n r) - e_r k_n u_n(z) H_1^{(1)}(k_n r)]. \end{aligned} \quad (4-28)$$

Using Eq. (4-26) for the derivative of a Hermite polynomial, we obtain

$$u_n'(z) = N_n k_a^{1/2} z_a^{-1/2} e^{-x^2/2} [2n H_{n-1}(x) - x H_n(x)]. \quad (4-29)$$

With Eq. (4-23) for Ψ_G , and Eqs. (4-28) and (4-29) for $\nabla\Psi_G$, the ray trace proceeds by solving $d\mathbf{r}/d\sigma = \text{Im}(\nabla\Psi/\Psi)$ numerically.

3. Exact ray analysis of a refractive waveguide

In this example we take the axis depth z_a to be 500 m and the sound speed on the axis, c_a , to be 1500 m/s. For a source frequency of 3 Hz, mode cutoff occurs at $n_c = \lfloor \pi - 1/2 \rfloor = 2$ by Eq. (4-27); the $n = 2$ mode propagates freely while the $n = 3$ mode attenuates exponentially with range. The low frequency and correspondingly low mode cutoff number ensure that the acoustic field will have simple behavior, and that any instabilities in the Hermite polynomial recursion relation will not have an opportunity to cause an accumulation of errors that might compromise the accuracy of the field calculation.

Figure 4.7 compares classical rays with exact rays for a source located on the sound channel axis ($z_0 = z_a = 500$ m). Since modes above cutoff may not be

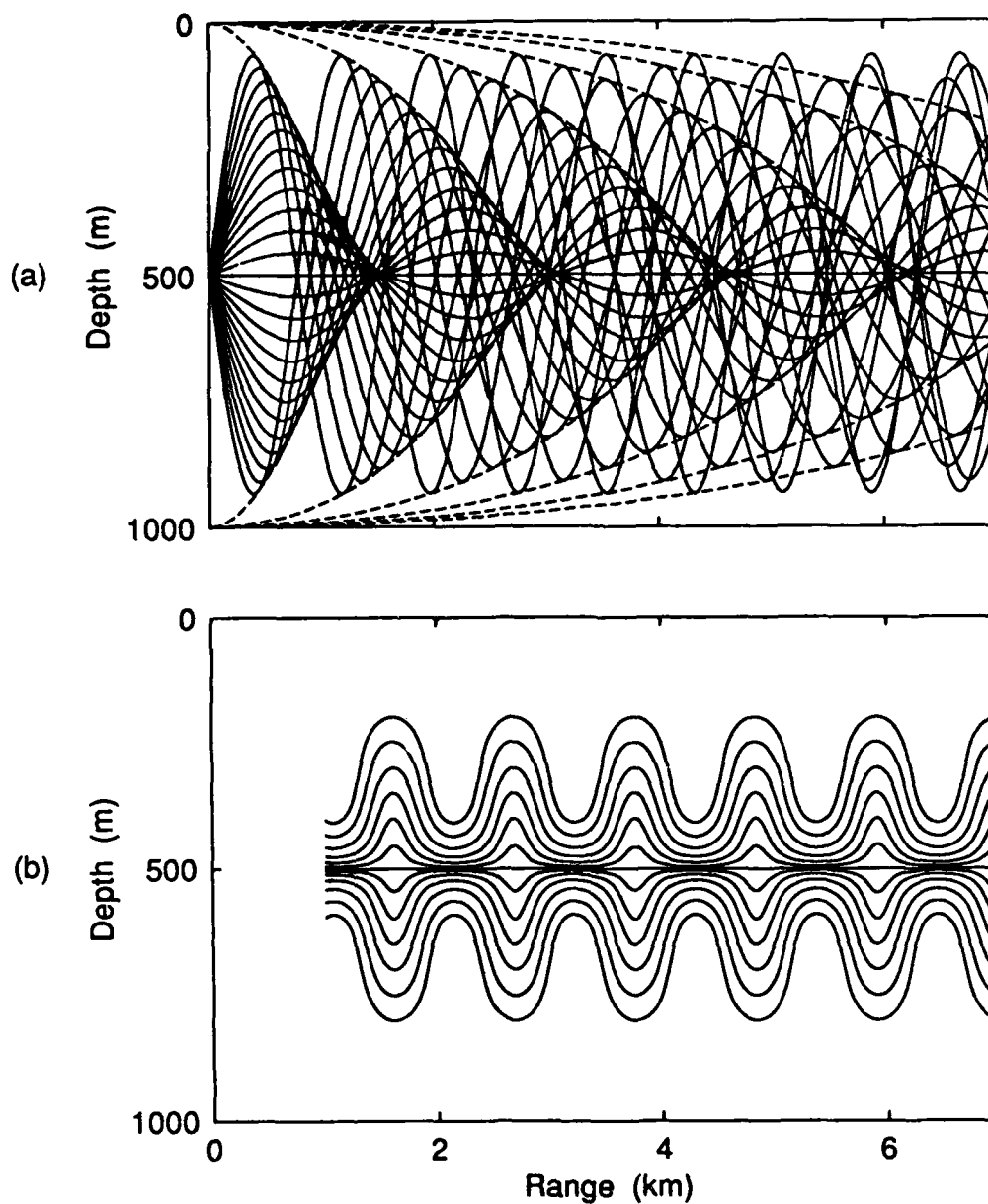


FIGURE 4.7 EXACT RAYS AND CLASSICAL RAYS IN THE HARMONIC OSCILLATOR WAVEGUIDE.
 (a) THE CLASSICAL RAYS (SOLID CURVES) FORM AN INFINITE SERIES OF CUSPED CAUSTICS
 (DASHED CURVES). (b) THE EXACT RAYS NEVER CROSS AND THEREFORE NEVER FORM CAUSTICS.

dropped from the mode summation until they have traveled far enough down the waveguide to damp out, exact ray traces must be confined to regions far enough from the source that the mode summation can be conveniently truncated with an acceptable truncation error. The exact ray traces depicted in Fig. 4.7(b) commence 1 km downrange from the source. The launch angles of these rays are not known and cannot readily be identified with their classical counterparts of Fig. 4.7(a); the ability to initiate the exact ray trace away from the source, as discussed in Sec. IV.A, is indispensable here.

The classical and exact rays are once again uncompromisingly different. Just as in the Kormilitsin problem of Sec. IV.D, the exact rays do not cross and form caustics, although they do concentrate in regions of high intensity. The classical rays do cross systematically and thus form an infinite series of cusped caustics, as shown in Fig. 4.7(a). The regions of greatest constriction of the exact ray bundles lie on the sound channel axis, but do not always coincide with the cusps of the classical ray caustics, where the acoustic field is most intense at high frequencies.

4. Phase velocity

The complex velocity potential $\varphi = Ae^{i\Phi - i\omega t}$ is explicitly time dependent. The phase speed c_{ph} is defined to be the rate ds/dt at which a point must advance along a ray path in order to keep the phase of φ constant at that point, where s is distance along the ray path. By requiring that the time derivative of $\Phi[s(t)] - \omega t$ vanish and by using $d\Phi/ds = K$, the phase speed is determined to be

$$c_{ph} = \omega/K. \quad (4-30)$$

In the ray theory approximation $k \approx K$,

$$c_{ph} \approx \omega/k = c.$$

In view of Eq. (4-30), the exact ray path equation

$$\frac{d}{ds} \left(K \frac{d\mathbf{r}}{ds} \right) = \nabla K$$

may be rewritten as

$$\frac{d}{ds} \left(\frac{1}{c_{ph}} \frac{d\mathbf{r}}{ds} \right) = \nabla \left(\frac{1}{c_{ph}} \right). \quad (4-31)$$

Conventional ray trace programs are based on the assumption that the sound speed and phase speed are synonymous; they solve Eq. (4-31) by assuming that $c_{ph} = c$. But even a conventional ray trace program would nevertheless trace out the exact ray paths if it were supplied the true phase speed (4-30) in place of the sound speed.

Figure 4.8 shows the level contours of the phase speed in the harmonic oscillator waveguide for different source depths and frequencies. The phase speeds were calculated using $c_{ph} = \omega/K$, with K obtained from Eq. (4-3). Phase speed contours

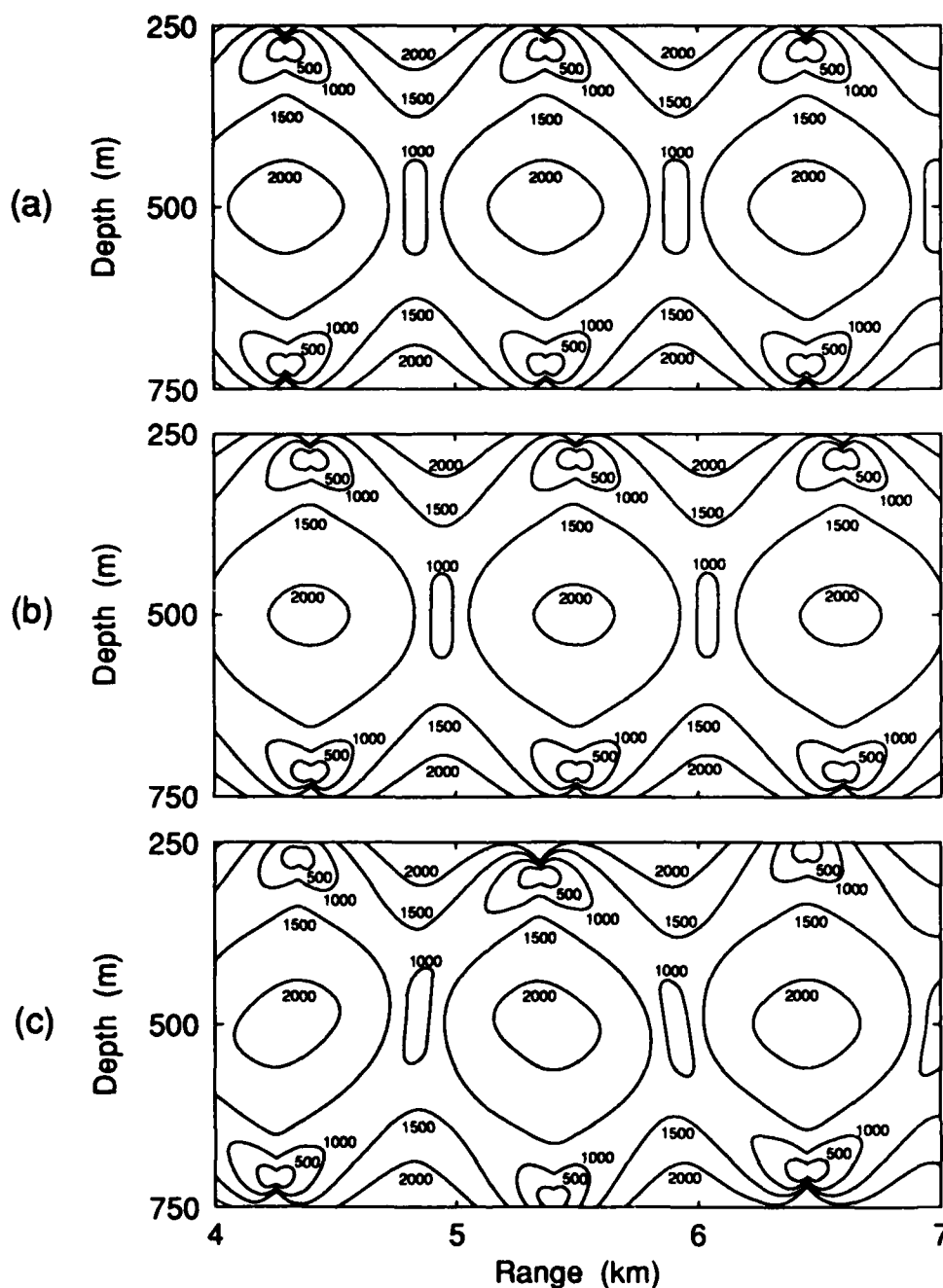


FIGURE 4.8 LEVEL CONTOURS OF THE PHASE SPEED $c_{ph} = \omega/K$. THE PHASE SPEED DEPENDS ON THE SOURCE DEPTH AND FREQUENCY. (a) $z_0 = 500$ m, $f = 3.0$ Hz. (b) $z_0 = 500$ m, $f = 3.1$ Hz. (c) $z_0 = 525$ m, $f = 3.0$ Hz.

for the 3 Hz source at 500 m are shown in Fig. 4.8(a). Notice that the phase speed is markedly range dependent even though the sound speed is range invariant. The phase speed contours shift when the frequency is raised slightly from 3.0 Hz to 3.1 Hz (Fig. 4.8[b]), and when the source depth is moved down slightly from 500 m to 525 m (Fig. 4.8[c]).

In general, K and the phase speed also depend on the source configuration and on the boundaries or radiation conditions. The frequency dependence of the phase speed is concomitant with the frequency dependence of the exact ray paths and with the dispersion observed in inhomogeneous media, even in the absence of boundaries.

We conclude the discussion of the harmonic oscillator waveguide with a further remark on the origin of its name. Hermite polynomials appear in eigenfunction solutions to the Schrödinger equation describing a quantum particle trapped in a conservative potential where the restoring force on the particle is proportional to its displacement from equilibrium (almost all quantum mechanics textbooks discuss this famous problem). In the classical limit, the particle undergoes time harmonic oscillations about its equilibrium position. The author chose the name "harmonic oscillator" waveguide to describe the waveguide which is the acoustic analog of the quantum harmonic oscillator.

G. FRAUNHOFER DIFFRACTION

We now take up the problem of a circular piston of radius a mounted flush in an infinite plane baffle. The farfield acoustic radiation exhibits Fraunhofer diffraction patterns.

1. Radiation from a circular piston in a baffle

In an unbounded homogeneous medium, the acoustic field at \mathbf{r} , due to a time harmonic point source at \mathbf{r}_0 , is

$$\Psi_G(\mathbf{r}; \mathbf{r}_0) = Q \frac{e^{ik|\mathbf{r}-\mathbf{r}_0|}}{|\mathbf{r}-\mathbf{r}_0|}. \quad (4-32)$$

To a good approximation, each elementary surface on the piston face radiates according to Eq. (4-32), so that the total acoustic field is given by an integration over the surface of the piston (we are exploiting the Huygens-Fresnel principle). The integration is most readily performed with the system configuration and coordinate system shown in Fig. 4.9. The baffle and the surface of the piston lie in the xy plane with the center of the piston at the origin. The piston radiates upward into the $z > 0$ region.

The integration over the piston surface is accomplished by resort to a farfield approximation. The diffraction patterns manifest only in the farfield, where $r \gg a$. The details of the calculation are given in many references on optics and acoustics

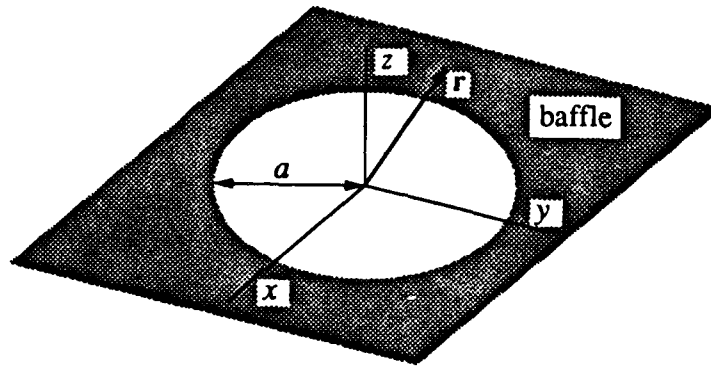


FIGURE 4.9 THE PISTON IN A BAFFLE. A CIRCULAR PISTON MOUNTED IN A PLANE BAFFLE CREATES FRAUNHOFER DIFFRACTION PATTERNS.

(see Kinsler and Frey[32] for an elementary discussion). The result is

$$\Psi(\mathbf{r}) = Q\pi a^2 \frac{e^{ikr}}{r} \frac{2J_1(ka \sin \theta)}{ka \sin \theta} \quad (4-33)$$

for the acoustic field far from the piston.

The directivity factor $2J_1(ka \sin \theta)/(ka \sin \theta)$ accounts for the Fraunhofer diffraction zones. The function $2J_1(x)/x$ is oscillatory, with an amplitude that falls off as $x^{-3/2}$ for large x . As expected, a beam of sound appears directly in front of the piston, where $\theta = 0$ and $2J_1(ka \sin \theta)/(ka \sin \theta)$ attains its maximum value of unity. But if the piston is large compared to a wavelength ($ka \gg 1$), then conical zones of enhanced intensity, due to diffraction, also form at angles corresponding to the extrema of $2J_1(ka \sin \theta)/(ka \sin \theta)$, interspersed with shadow zones corresponding to the zeros of $J_1(ka \sin \theta)$. On the other hand, if the piston is on the order of a wavelength across ($ka \sim 1$), then no shadow zones or secondary maxima appear. If the piston is small ($ka \ll 1$), then the primary beam is greatly dispersed, radiating with nearly uniform intensity in all directions from the piston.

When secondary maxima are present they are far less intense than the primary. At any fixed distance r from the piston, the peak intensity in the first diffraction zone is 17.5 dB below that of the central maximum; the peak intensity of the second zone is 23.8 dB down.

2. Diffraction of exact rays

Upon taking the gradient of Ψ (Eq. [4-33]), we discover that

$$\frac{\nabla \Psi}{\Psi} = \left(ik - \frac{1}{r} \right) \frac{\mathbf{r}}{r},$$

which is the same result obtained in the case of the point source in an unbounded homogeneous medium (see Sec. IV.B). The reader will recall that, in that case, the ray paths were radial lines originating at the origin. Here, our conclusions are restricted

to the farfield, where the ray paths are once again found to be radial lines, with retrograde projections back to the origin. (However, we do not know the paths the rays followed through the nearfield to get to the farfield.)

The field amplitude, obtained from $A^2 = \Psi\Psi^*$, is

$$A = \frac{2\pi Qa^2}{r} \left| \frac{J_1(ka \sin \theta)}{ka \sin \theta} \right|,$$

which is to be compared with $A = 1/r$ for the point source. Clearly these diffracted radial rays do not all bear equal energy, as they did in the unbounded medium, but have intensities appropriate to their positions in the diffraction pattern.

The piston problem illustrates several interesting properties of exact ray theory. It demonstrates, as did the harmonic oscillator waveguide case, that fruitful ray analysis can sometimes proceed even when there are large regions where the ray paths cannot be computed. In exact ray theory, problem areas may sometimes be "skipped over," whereas in classical ray theory, ray traces must usually proceed from the source without interruption.

The piston problem involved a distributed source, an often problematical situation for classical ray theory because it is not always clear how to initiate the ray trace. In the exact ray theory analysis we simply stepped over the troublesome nearfield and took advantage of knowledge of the farfield results.

The method of analysis of the piston problem is also applicable to the problem of a plane wave normally incident on a circular hole in a baffle. If the hole is not so small that $ka \ll 1$, then the acoustic field in the hole may be taken to be that of the incident field (the Kirchhoff approximation) and the analysis proceeds as it did for the piston problem. According to classical ray theory, the rays passing through the hole do not diverge, but form a beam of parallel rays. The acoustic field is uniform across this beam and vanishes abruptly at the edge of the beam. By contrast, exact ray analysis accounts for diffraction by predicting diverging rays of variable intensity.

H. BEAM DISPLACEMENT AND REFLECTIONS FROM A BOUNDARY

Until recently most computer implementations of ray theory have treated acoustic interaction with the surface and bottom boundaries in a rather simplistic fashion, letting the rays reflect in the specular direction and imposing a plane wave reflection loss and phase shift, and possibly a frequency dependent rough scattering loss. This approach works quite well when applied to a smooth ocean surface, because then the surface is an almost perfect pressure release boundary; the rays reflect in the specular direction with a 180° phase shift and undiminished amplitude. (Attempts to treat scattering from a rough sea surface have had mixed success.) The method meets with indifferent to poor success when applied to bottom interaction. It is notoriously inadequate in shallow water, where bottom interacting energy can dominate the propagation problem.

The lateral displacement of a bounded beam reflecting from an interface is a well known phenomenon.[33] In 1981, Tindle and Bold[34] published their discovery

that ray theory calculations could be made very accurate, even in shallow water, by imposing a beam displacement and phase shift on bottom reflected rays, so that the reflected ray emerged from the bottom somewhat displaced from its point of incidence (see Fig. 4.10), and with an additional phase shift imposed.

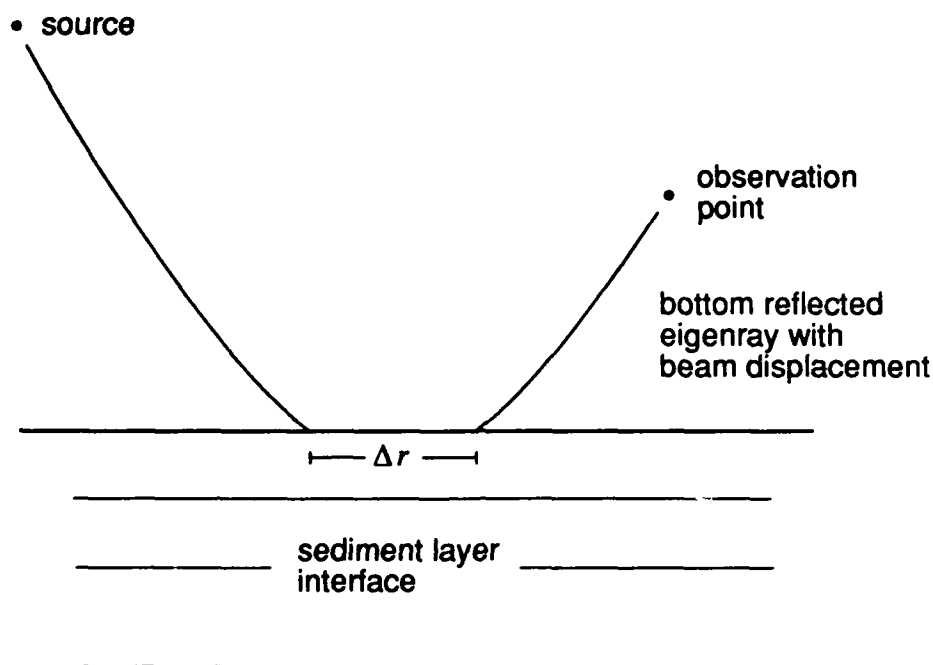


FIGURE 4.10 BEAM DISPLACEMENT OF A BOTTOM REFLECTED RAY.

Implementation of beam displacement in a computer ray model is straightforward. The complex plane wave reflection coefficient $V(\theta)$ is computed for a ray incident on the bottom at grazing angle θ in the usual fashion. But the point of origin of the reflected ray is displaced from the point of incidence by a distance Δr given by

$$\Delta r = \frac{1}{k_b \sin \theta} \frac{\partial \phi}{\partial \theta}, \quad (4-34)$$

where k_b is the wave number in the water at the bottom interface, and ϕ is the phase of V . There is also a beam displacement phase shift $\Delta\Phi_b$ given by

$$\Delta\Phi_b = k_b \Delta r \cos \theta$$

in addition to the bottom reflection phase shift directly attributable to V . Caustics will usually be created by including beam displacements even if none were present before, and these must be treated by uniform asymptotics. Curiously, the phase shift accrued by a ray which grazes a beam displacement caustic is $\pi/2$ (a phase *lead*) instead of the familiar $-\pi/2$ phase lag from encountering a conventional caustic.

All of these seemingly peculiar manipulations have been shown to be mathematically well justified.[33,35] Batorsky and Felsen[36] showed that beam displacements

are inherent in the transformation from normal mode to ray theory representations when a bottom is present. And there are compelling computational reasons for preferring a ray calculation to a normal mode calculation, even though the normal mode result is slightly more accurate: ray theory models can easily treat broadband sources and sloping bottoms. Even so, beam displacement seems to many to be an ad hoc correction with several counterintuitive properties, and this has discouraged its use.

Heading the list of disquieting properties is the fact that a *single* beam-displaced eigenray can emerge from the bottom and properly account for the bottom interaction effects of an ocean bottom consisting of *several* partially reflecting sediment layer interfaces. Experience with classical ray theory suggests that rays should split at the interfaces to account for the partial reflection and transmission of energy, and that this should result in a large, or even infinite number of eigenrays emerging from the bottom. This notion of how the rays should behave persists even though this model of bottom interaction produces poor predictions. Then again, the computer modeler *can* elect to use a split-ray approach, but with beam displacements imposed on every partially reflected ray,[37] although the split-ray approach complicates the modeler's task. The reader has probably already begun to suspect that this single eigenray/multiple eigenray quandary is another manifestation of the confounding of cw and broadband phenomena.

1. Reflection from a boundary

If a point source is located above a rigid perfect reflector as shown in Fig. 4.11, then the acoustic field is given by

$$\Psi(r, z; z_0) = \Psi_{\text{sphere}} + \Psi_{\text{refl}}, \quad (4-35)$$

where

$$\Psi_{\text{sphere}} = \frac{e^{ikR}}{R}, \quad \Psi_{\text{refl}} = \frac{e^{ikR_1}}{R_1},$$

and

$$R^2 = r^2 + (z - z_0)^2, \quad R_1^2 = r^2 + (z + z_0)^2$$

(the source strength has been dropped in Eq. [4-35]). Classical ray theory yields the exact solution to the Helmholtz equation in this case, and the two classical eigenrays are shown in Fig. 4.11. The direct path eigenray connects the source at $(0, z_0)$ with the observation point at (r, z) . The bottom reflected eigenray may be replaced by an equivalent ray which connects the source image at $(0, -z_0)$ with the observation point.

If we proceed to trace the exact eigenray by solving $dr/d\sigma = \text{Im } \nabla \Psi / \Psi$, as we have in all the previous sections, the result is the wavy curve shown in Fig. 4.11. (This exact eigenray, incidentally, was traced *backwards* from the observation point to the source.) Two classical eigenrays are replaced by a single exact eigenray in the usual fashion, but the result does not seem particularly illuminating.

A more fruitful approach is suggested by the representation of the total field in Eq. (4-35) as a superposition of a spherical wave and a reflected wave field. Each

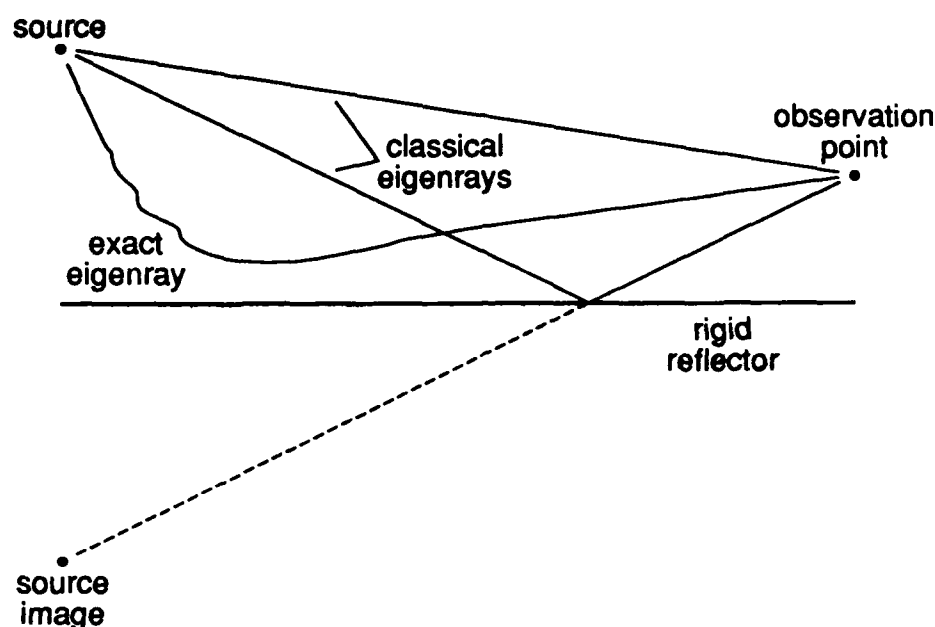


FIGURE 4.11 REFLECTION FROM A RIGID BOUNDARY. THE CLASSICAL EIGENRAYS (SOLID STRAIGHT LINE SEGMENTS) MAY BE REPLACED BY A SINGLE EXACT EIGENRAY (WAVY CURVE).

of the contributing wave fields can be represented separately by an exact eigenray. Thus the exact eigenray representing Ψ_{sphere} is the usual straight line from source to observation point. The exact ray representing Ψ_{refl} connects the source image point with the observation point; it is the equivalent of the bottom reflected ray of classical ray theory. The exact and classical eigenrays coincide, of course, because classical ray theory is exact in this case. The representation of the acoustic field by two terms, each with its own exact ray representation, is the key to establishing the connection between exact ray theory and beam displacement.

The phenomenon of beam displacement manifests itself only when the reflecting boundary is not a perfect reflector. We will treat the simplest such case: that of a point source in a homogeneous fluid half-space overlying another homogeneous half-space. The total field is again written as the sum of a spherical wave field and a reflected field, and Ψ_{sphere} is computed as before. To compute the reflected field the spherical wave impinging on the interface is expanded in terms of plane waves (the expansion takes the form of an integral over the grazing angles). The reflected field is then obtained by computing the reflected plane wave corresponding to each incident plane wave by application of a plane wave reflection coefficient. The contributions of the reflected plane waves are integrated by a saddle point approximation. The calculation is lengthy; fortunately, the details are supplied by Brekhovskikh,[33] pp. 242-255, and we need only state the results:

$$\Psi_{\text{refl}} = Q \frac{e^{ikR_1}}{R_1},$$

$$\begin{aligned}
Q &= V(\theta) - iM(\theta, R_1), \\
M &= N(\theta)/kR_1, \\
N &= \frac{1}{2}[V''(\theta) - V'(\theta) \tan \theta], \\
\tan \theta &= (z + z_0)/r,
\end{aligned} \tag{4-36}$$

which are valid for $kR \gg 1 \ll kR_1$ and for grazing angles θ not closely approaching the critical angle θ_{cr} below which total internal reflection occurs. Primes denote differentiation with respect to the grazing angle θ (Brekhovskikh works with the angle of incidence, which accounts for the differences between the formulas in the reference and those appearing here).

The logarithmic derivatives of Ψ required for ray tracing are

$$\begin{aligned}
\frac{\partial \Psi_{\text{refl}}/\partial r}{\Psi_{\text{refl}}} &= \frac{\partial Q/\partial r}{Q} + (ikR_1 - 1) \frac{\partial R_1/\partial r}{R_1}, \\
\frac{\partial \Psi_{\text{refl}}/\partial z}{\Psi_{\text{refl}}} &= \frac{\partial Q/\partial z}{Q} + (ikR_1 - 1) \frac{\partial R_1/\partial z}{R_1},
\end{aligned} \tag{4-37}$$

where

$$\begin{aligned}
\partial Q/\partial r &= [irM - (z + z_0)(V' - iN'/kR_1)]/R_1^2, \\
\partial Q/\partial z &= [i(z + z_0)M + r(V' - iN'/kR_1)]/R_1^2,
\end{aligned}$$

and

$$\begin{aligned}
\partial R_1/\partial r &= r/R_1, \\
\partial R_1/\partial z &= (z + z_0)/R_1.
\end{aligned}$$

Equations (4-36) and (4-37) are valid regardless of the complexity of the ocean bottom.

In the case of the fluid half-space bottom, the plane wave reflection coefficient $V(\theta)$ is given by

$$V = \frac{\rho_1 \sin \theta - \rho(n^2 - \cos^2 \theta)^{1/2}}{\rho_1 \sin \theta + \rho(n^2 - \cos^2 \theta)^{1/2}}, \tag{4-38}$$

where ρ and c are the density and sound speed in the upper half-space, ρ_1 and c_1 are the density and sound speed in the lower half-space, and $n = c/c_1$. In this instance, V is independent of frequency. The beam displacement, computed according to Eq. (4-34), is zero unless the grazing angle is less than the critical angle, given by

$$\cos \theta_{cr} = n.$$

By letting $m = \rho_1/\rho$ and defining

$$\alpha = m \sin \theta, \quad \beta = m \cos \theta, \quad \gamma = (n^2 - \cos^2 \theta)^{1/2},$$

the required derivatives of V and N are found to be

$$\begin{aligned} V' &= \frac{\beta(1-V) - \gamma'(1+V)}{\alpha + \gamma}, \\ V'' &= -\frac{\alpha(1-V) + \gamma''(1+V) + 2(\beta + \gamma')V'}{\alpha + \gamma}, \\ V''' &= -\frac{\beta(1-V) + \gamma'''(1+V) - 3(\alpha - \gamma'')V' + 3(\beta + \gamma')V''}{\alpha + \gamma}, \\ N' &= \frac{1}{2}(V''' - V'' \tan \theta - V' \sec^2 \theta), \end{aligned}$$

where

$$\begin{aligned} \gamma' &= \frac{\alpha\beta}{m^2\gamma}, \\ \gamma'' &= \frac{\beta^2 - \alpha^2 - (m\gamma')^2}{m^2\gamma}, \\ \gamma''' &= -\gamma'(4 + 3\gamma''/\gamma). \end{aligned}$$

2. Frequency dependent ray representation of beam displacement

Since the calculation of Ψ_{ref} relies on a saddle point approximation the resulting rays are not quite exact rays. Nor are they frequency dependent rays, since the reflection coefficient V , given by Eq. (4-38), is frequency independent. Rather than engage in a pointless search for a suitable qualifying adjective I shall simply continue to call these exact rays.

Figure 4.12(a) shows a point source located 100 m above a plane interface, and an observation point located 50 m above the interface and 450 m downrange from the source. The fluid density ratio is $\rho_1/\rho = 1.25$ and the sound speed ratio is $n = c/c_1 = 1500/1750$. The solid straight line segments are the classical direct path and bottom reflected eigenrays. The broken line is the bottom interacting eigenray with beam displacement included (the beam displacement was computed according to Eq. [4-34]).

Figure 4.12(b) shows the frequency dependent eigenray for Ψ_{ref} , which was traced backwards from the observation point until it intersected the interface. The classical eigenrays are drawn in for comparison. *The frequency dependent eigenray for the reflected field coincides almost exactly with that segment of the beam displaced eigenray which connects the bottom with the observation point, even though the methods used to compute the exact ray and the beam displaced ray are quite different.*

The homogeneous half-space bottom was chosen for the sake of simplicity, but the substitution of a more complicated bottom would merely change the details. Once the decision is made to represent the total field as a superposition of a waterborne field and a bottom reflected field (and this is always permissible), then the waterborne and reflected fields at an observation point can always be represented separately by their

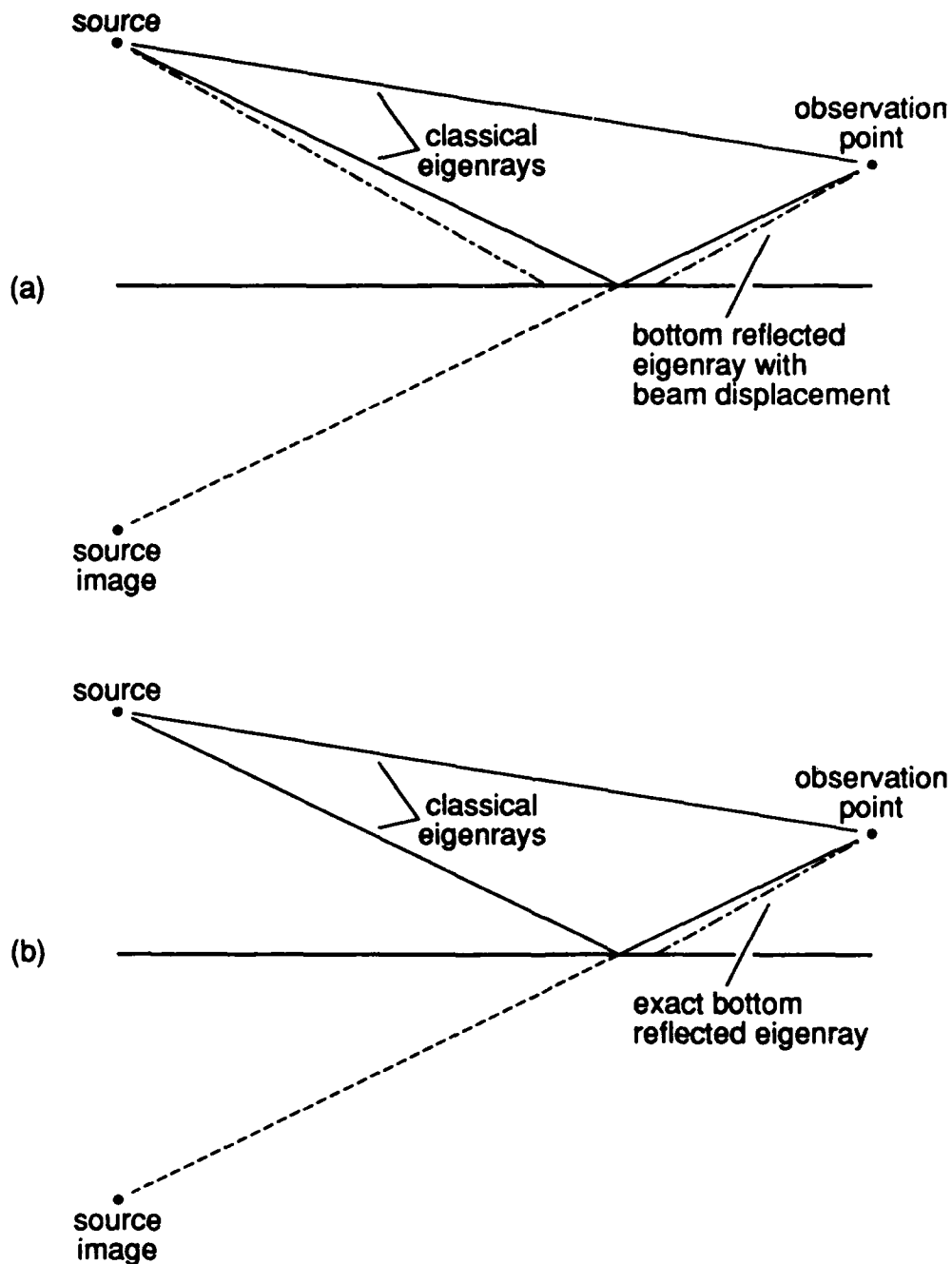


FIGURE 4.12 BEAM DISPLACEMENT. (a) THE SOLID STRAIGHT LINE SEGMENTS ARE THE CLASSICAL EIGENRAYS. THE BROKEN LINE IS THE BOTTOM REFLECTED EIGENRAY WITH BEAM DISPLACEMENT. (b) THE FREQUENCY DEPENDENT EIGENRAY REPRESENTING THE REFLECTED FIELD, SHOWN WITH THE CLASSICAL RAYS FOR REFERENCE.

respective frequency dependent eigenrays. Moreover, there will always be exactly one eigenray to account for bottom interaction in this representation no matter how complicated the bottom and, in particular, no matter how many sediment layer interfaces there are. And that eigenray will ordinarily exhibit a displacement.

On the other hand, it is also permissible to write the reflected field as a superposition of reflected fields from each layer interface in the bottom. In that case, each of these layers may be represented by its own frequency dependent eigenray, each with its own displacement. Thus both approaches to implementing beam displacement in a classical ray model are vindicated.

It is important to note that the displacement of the bottom reflected frequency dependent eigenray appeared naturally; it was not necessary to introduce it, as is the case in conventional ray tracing.

I. EXACT RAY THEORY AND MULTIPATHING

We saw in the previous section that frequency dependent ray diagrams could be constructed for each term in the two-term representation of the field for a source above a partially reflecting boundary. In the case examined, the field at an observation point was given by the coherent addition of two frequency dependent eigenrays, one being a direct path ray from the source to the observation point, and the other emerging from the bottom (see Fig. 4.12[b]). Although the field could also be represented by a single frequency dependent eigenray, as in Fig. 4.11, it proved more illuminating to construct two frequency dependent eigenrays. By drawing both rays on the same ray diagram we reintroduce a form of multipathing.

In general, if an expression for the acoustic field takes the form of a series, then each term in the series may be represented by its own ray diagram. Such term-by-term representations of the field can be illuminating, as we have just seen. If the diagrams are combined so that all of the rays appear on the same diagram, then the rays will generally cross and a semblance of multipathing appears. But the fact that a ray from one diagram might cross or graze a ray from another diagram should not cause alarm that the transport equation is poised once again to predict singularities at caustics. Each ray diagram is actually independent of all the others. No single ray diagram will exhibit multipathing, and the transport equation must be applied separately to each diagram.

When multipathing is introduced in this way the exact eigenrays have the peculiar property that not all of them can be traced back to the original source. The example of beam displacement examined in the last section showed an exact ray apparently emerging from the bottom, but it is quite meaningless to inquire how the ray "got there." The harmonic oscillator waveguide supplies another example. In that case, the acoustic field was expressed as a normal mode summation. We can now see that each term in that series would have its own exact ray representation and, in fact, the behavior of those rays is easily discerned. The rays for each term in the series are simply horizontal lines projecting from the z axis. The z axis acts as a line source for these rays even though the actual source was a point. We find that $K = k_n$ for

58

the n th term, where k_n^2 is the eigenvalue for that term and mode.

V. CONCLUSION

The computational convenience and physical insight provided by ray theory models have encouraged their use even under conditions where the approximation inherent in the theory becomes a serious liability. In underwater acoustics, for example, ray models are used increasingly in long range, low frequency propagation analysis, and in shallow water propagation analysis. But in these environments, ray theory deficiencies in the treatment of caustics, bottom interaction, and weakly ducted propagation detract from its usefulness. In an effort to retain the advantages of ray theory while correcting its lapses, researchers have developed several wave theoretical corrections to classical ray theory.

The author has been engaged for several years in applying ray theory to the Helmholtz equation which describes the acoustic field generated by a time harmonic source. During the doctoral research which led to this dissertation, I became intrigued by the possibility that the ray theory approximation might be abolished altogether in solutions to the Helmholtz equation. The idea was to recast the Helmholtz equation in a ray theoretical formulation in which a geometrical energy conservation law (the transport equation) would be obeyed *exactly*. The reformulation in fact turned out to be very straightforward, but did not lead to a practical computational scheme for solving the Helmholtz equation. What did emerge, however, was a practical computational method for constructing exact ray diagrams from known solutions to the Helmholtz equation. Thus, whenever a solution to the Helmholtz equation is available, whether by analytical or numerical methods, the solution may be represented in the form of an exact ray diagram. The transport of energy within the flux tubes formed by exact ray paths is rigorously conservative; the ratio of areas law, familiar from classical ray theory, which governs intensity in infinitesimal ray bundles ceases to be an approximation.

Yet, in a series of numerical experiments described in this dissertation, the exact ray diagrams constructed for several known solutions to the Helmholtz equation are utterly unlike the corresponding classical ray diagrams. This is so despite the fact that classical ray theory makes quite accurate field predictions for most of these cases, provided allowances are made for caustics and other known problematical regions. Moreover, the differences are not reconciled at high frequencies, as might be expected. The surprising fact is that, by expunging the ray theory approximation altogether, the character of the ray paths is changed completely. Actually, several principal features of exact ray diagrams had been anticipated long before methods were invented for tracing exact rays, but that hardly abated the sense of surprise upon eventual confirmation.

The lack of multipathing is the single feature which most distinguishes exact ray diagrams from their classical counterparts. The explanation for this difference goes directly to the nature of classical ray theory and the ray theory approximation. It is

shown that classical ray theory is based on the phenomenology of propagating fronts generated by pulsed sources, while exact ray theory is founded on the phenomenology of time harmonic fields. When classical ray theory is applied, somewhat out of its natural context, to the Helmholtz equation, it takes the form of a *nonuniform* high frequency asymptotic approximation. The nonuniformity largely accounts for the differences between classical and exact ray theory.

As to practical considerations, even though exact ray theory does not presently offer any improved computational methods, it does provide a new method for displaying the acoustic field. If the new ray diagrams were merely minor perturbations of the classical ray diagrams then they would be of little interest. But because exact ray diagrams are usually profoundly different from classical diagrams, they can provide insights offered by no other method of display. The computational method for tracing exact rays lends itself to implementation in existing numerical propagation models. Suitably modified models would be capable not only of predicting the amplitude and phase of the acoustic field but also of tracing out its lines of propagation.

REFERENCES

1. Philip M. Morse and Herman Feshbach, *Methods of Theoretical Physics* (McGraw-Hill, New York, 1953).
2. C. Allan Boyles, *Acoustic Waveguides: Applications to Oceanic Science* (Wiley, New York, 1984).
3. L. B. Dozier and F. D. Tappert, "Statistics of normal mode amplitudes in a random ocean, I. Theory," *J. Acoust. Soc. Am.* **63**, 353-365 (1978).
4. M. Cecile Penland, *The Effects of Internal Waves on Acoustic Normal Modes* (Ph.D. dissertation, The University of Texas at Austin, 1984).
5. J. Lighthill, *Waves in Fluids* (Cambridge University Press, New York, 1978), pp. 1-3.
6. S. R. Rutherford and K. E. Hawker, "Effects of density gradients on bottom reflection loss for a class of marine sediments," *J. Acoust. Soc. Am.* **63**, 750-757 (1978).
7. Robert J. Urick, *Principles of Underwater Sound for Engineers* (McGraw-Hill, New York, 1967), pp. 94-104.
8. A. Sommerfeld and J. Runge, "Application of vector calculus to the fundamentals of geometrical optics," *Ann. Phys.* **35** (4), 277-298 (1911).
9. Edward R. Floyd, "Modified phase integral approximation for a more rigorous ray-tracing technique," *J. Acoust. Soc. Am.* **60** (4), 801-809 (1976).
10. C. B. Officer, *Introduction to the Theory of Sound Transmission, with Application to the Ocean* (McGraw-Hill, New York, 1958), pp. 36-40.
11. Herbert Goldstein, *Classical Mechanics* (Addison-Wesley, Reading, Mass., 1950; second edition, 1980).
12. L. D. Landau and E. M. Lifshitz, *Mechanics* (Pergamon Press, New York, 1976).
13. C. W. Horton, Sr. "Dispersion relationships in sediments and sea water," *J. Acoust. Soc. Am.* **55**(3), 547-549 (1974).
14. M. O'Donnell, E. T. Jaynes, and J. G. Miller, "General relationships between ultrasonic attenuation and dispersion," *J. Acoust. Soc. Am.* **63**(6), 1935-1937 (1978).
15. E. B. Christoffel, *Ann. Math.* **8**, 81 (1877).

16. R. K. Luneburg, "Mathematical theory of optics," Brown University (1944), "Propagation of electromagnetic waves," New York University (1949).
17. G. S. Heller, "Propagation of acoustic discontinuities in an inhomogeneous moving liquid medium," *J. Acoust. Soc. Am.* **25**, 938-947 (1953).
18. Joseph B. Keller, "Geometrical acoustics. I. The theory of weak shock waves," *J. Acoust. Soc. Am.* **25**, 950-951 (1953).
19. R. Pitre, *On the Application of Horizontal Ray Theory to Acoustic Propagation in the Ocean Waveguide* (Ph.D. dissertation, The University of Texas at Austin, 1984).
20. K. C. Chen and Donald Ludwig, "Calculation of wave amplitudes by ray tracing," *J. Acoust. Soc. Am.* **54**, 431-436 (1973).
21. E. Fehlberg, "Klassische Runge-Kutta-Formeln vierter und niedrigerer Ordnung mit Schrittweiten-Kontrolle und ihre Anwendung auf Wärmeleitungsprobleme," *Computing* **6**, 61-71 (1970).
22. John J. Cornyn, *GRASS: A Digital-Computer Ray-Tracing and Transmission-Loss-Prediction System*, NRL Report No. 7621, Vol. 1, Naval Research Laboratory, Washington D.C. (1973).
23. T. L. Foreman, *Ray Modeling Methods for Range Dependent Ocean Environments*, ARL Technical Report No. 83-41, Applied Research Laboratories, The University of Texas at Austin (1983).
24. R. Michael Jones, J. P. Riley, T. M. Georges, *HARPO: A Versatile Three-Dimensional Hamiltonian Ray-Tracing Program for Acoustic Waves in an Ocean with Irregular Bottom*, Wave Propagation Laboratory, Boulder, Colorado (1986).
25. C. L. Pekeris, "Theory of propagation of sound in a halfspace of variable sound velocity under conditions of formation of a shadow zone," *J. Acoust. Soc. Am.* **18**, 295-315 (1946).
26. B. T. Kormilitsin, "Propagation of electromagnetic waves in a medium with dielectric constant $\epsilon(\mathbf{z}) = \epsilon_0 + \epsilon_1(\mathbf{z})$ excited by a source in the form of a luminescent filament," *Radio Eng. Electron Phys. (USSR)* **11**, 988-992 (1966).
27. R. L. Holford, "Elementary source-type solutions of the reduced wave equation," *J. Acoust. Soc. Am.* **70**(5), 1427-1436 (1981).
28. D. Ludwig, "Uniform asymptotic expansions at a caustic," *Commun. Pure Appl. Math.* **19**, 215-250 (1966).

29. Y. A. Kravtsov, "One modification of the geometric optics method," *Sov. Radiophys.* **7**(4), 104-117 (1964).
30. Milton Abramowitz and Irene A. Stegun, *Handbook of Mathematical Functions* (Dover, New York, ninth printing, 1970), pp. 446-456.
31. D. White and M. Pedersen, "Evaluation of shadow-zone fields by uniform asymptotics and complex rays," *J. Acoust. Soc. Am.* **69**(4), 1029-1059 (1981).
32. Lawrence E. Kinsler and Austin R. Frey, *Fundamentals of Acoustics*, 2nd ed. (Wiley, New York, 1962), pp. 166-183.
33. L. Brekhovskikh, *Waves in Layered Media* (Academic Press, New York, 1960, and second edition, 1980).
34. C. T. Tindle and G. J. Bold, "Ray calculations with beam displacement," *J. Acoust. Soc. Am.* **70**(3), 813-819 (1981).
35. D. C. Stickler, D. S. Ahluwalia, and L. Ting, "Application of Ludwig's uniform progressing wave ansatz to a smooth caustic," *J. Acoust. Soc. Am.* **69**, 1673-1681 (1981).
36. D. V. Batorsky and L. B. Felsen, "Ray-optical calculation of modes excited by sources and scatterers in a weakly inhomogeneous duct," *Radio Sci.* **6**, 911-923 (1971).
37. E. K. Westwood and P. J. Vidmar, "Eigenray finding and time series simulation in a layered-bottom ocean," *J. Acoust. Soc. Am.* **81** (4), 912-924 (1987).

28 March 1988

DISTRIBUTION LIST FOR
ARL-TR-88-17
UNDER CONTRACT N00014-87-K-0346

Copy No.

1 Commanding Officer
2 Naval Ocean Research and Development Activity
3 Stennis Space Center, MS 39529-5000
4 Attn: B. Adams (Code 110A)
5 J. Matthews (Code 222)
6 D. Del Balzo (Code 244)
7 R. Wagstaff (Code 425)
8 H. Ali (Code 425)
9 J. Caruthers (Code 220)
10 T. Goldsberry (Code 240)
11 P. Valent (Code 363)
12 C. Salinger (Code 222)
13 D. Lavoie (Code 363)
14 W. Moseley (Code 200)
15 Library

13 Office of Naval Research Field Detachment
14 Stennis Space Center, MS 39529-5000
Attn: E. D. Chaika (Code 132)
B. N. Wheatley (Code 132)

15 Office of the Chief of Naval Research
16 Department of the Navy
17 Arlington, VA 22217-5000
18 Attn: G. L. Johnson (Code 1125)
19 R. Fitzgerald (Code 1125OA)
20 R. Jacobson (Code 1125GG)
21 J. H. Kravitz (Code 1125GG)
R. F. Obrochta (Code 1221)
G. Gotthardt (Code 1321)
B. Blumenthal (Code 1322)

22 Chief of Naval Research
Office of Naval Technology
Department of the Navy
Arlington, VA 22217-5000
Attn: J. T. Warfield (Code 234)

Distribution List for ARL-TR-88-17 under Contract N00014-87-K-0346
(cont'd)

Copy No.

23 Commander
24 Space and Naval Warfare Systems Command
25 Department of the Navy
26 Washington, D.C. 20363-5100
Attn: L. Parish (PMW180-4)
K. Hawker (PMW180-4)
R. Mitnick (PMW180-4)
D. Doolittle (PMW180-4)

27 Commander
28 Naval Sea Systems Command
29 Department of the Navy
30 Washington, D.C. 20363-5101
Attn: P. Tiedeman (Code 63D3)
M. Schultz (Code 63D7)
Y. Yam (Code 63D4)
E. Plummer (Code 63D1)

31 Commander
Naval Air Systems Command
Department of the Navy
Washington, D.C. 20361-5460
Attn: W. Parigian (Code 933B)

32 Director
33 Naval Research Laboratory
34 Washington, D.C. 20375
35 Attn: Library
36 O. Diachok (Code 5120)
37 M. F. Czarnecki (Code 5110)
F. Ingenito (Code 5160)
D. Bradley (Code 5100)
R. Gragg (Code 5160)
R. Pitre (Code 5160)

Distribution List for ARL-TR-88-17 under Contract N00014-87-K-0346
(cont'd)

Copy No.

	Commanding Officer Naval Ocean Systems Center San Diego, CA 92152-5000
38	Attn: Library
39	H. Bucker (Code 541)
40	C. Persons (Code 732)
41	F. Ryan (Code 541)
42	D. Hanna (Code 702)
	Chief of Naval Operations U. S. Naval Observatory Washington, D.C. 20390
43	Attn: CDR R. Hillyer (Code 006D3)
	Office of the Chief of Naval Operations Department of the Navy Arlington, VA 20350
44	Attn: A. Bisson (OP213T)
	Commander Naval Surface Warfare Center White Oak Laboratory Silver Spring, MD 20910
45	Attn: Library
	Commander David Taylor Research Center Bethesda, MD 20034
46	Attn: Library
	Commanding Officer Naval Oceanographic Office Stennis Space Center, MS 39522-5001
47	Attn: Library
48	W. Jobst (Code 7300)
49	R. Hecht (Code 7310)

Distribution List for ARL-TR-88-17 under Contract N00014-87-K-0346
(cont'd)

Copy No.

	Commanding Officer Naval Air Development Center Warminster, PA 18974
50	Attn: Library
51	B. Steinberg (Code 5031)
	Officer in Charge Naval Underwater Systems Center New London Laboratory New London, CT 06320
52	Attn: Library
53	P. Herstein (Code 33A3)
54	R. Deavenport (Code 3332)
55	W. Carey (Code 33A)
56	D. Lee (Code 3342)
57	B. Cole (Code 33A)
58	J. J. Hanrahan
	Superintendent Naval Postgraduate School Monterey, CA 93943
59	Attn: Library
60	H. Medwin (Dept. of Physics)
	Commanding Officer Naval Coastal Systems Center Panama City, FL 32407
61	Attn: Library
62	G. McLeroy
	Defense Advanced Research Projects Agency Arlington, VA 22209
63	Attn: C. Stuart
64	Commanding Officer Naval Intelligence Support Center Washington, D.C. 20390

Distribution List for ARL-TR-88-17 under Contract N00014-87-K-0346
(cont'd)

Copy No.

65 - 76

Commanding Officer and Director
Defense Technical Information Center
Cameron Station, Building 5
5010 Duke Street
Alexandria, VA 22314

Woods Hole Oceanographic Institution
86-95 Water Street
Woods Hole, MA 02543

77
78
79

Attn: R. Spindel
J. Lynch
G. Frisk

Science Applications, Inc.
1710 Goodridge Drive
McLean, VA 22101

80
81
82
83

Attn: C. Spofford
J. Hanna
W. Monet
P. Rost
P. Vidmar

Applied Research Laboratory
The Pennsylvania State University
P.O. Box 30
State College, PA 16801

84
85
86
87

Attn: Library
S. McDaniel
D. McCammon
F. Beebe

Applied Physics Laboratory
The University of Washington
1013 N.E. 40 St.
Seattle, WA 98105

88

Attn: Library

Distribution List for ARL-TR-88-17 under Contract N00014-87-K-0346
(cont'd)

Copy No.

89	Marine Physical Laboratory Scripps Institution of Oceanography The University of California, San Diego San Diego, CA 92093 Attn: F. H. Fisher
90	Bell Telephone Laboratories, Inc. Whippany Road Whippany, NJ 07961 Attn: A. Carter R. Patton Library
91	
92	
93	Planning Systems, Inc. 7900 Westpark Drive McLean, VA 22101 Attn: R. Cavanaugh B. Brunson
94	
95	Planning Systems, Inc. 115 Christian Lane Slidell, LA 70458 Attn: J. Paquin M. Bradley W. Geddes
96	
97	
98	Daubin Systems Corporation 104 Crandon Blvd. P. O. Box 49-0249 Key Biscayne, FL 33149 Attn: Lan Nghiem-Phu
99	TRW, Inc. TRW Defense & Space Systems Group Washington Operations 7600 Colshire Drive McLean, VA 22101 Attn: R. T. Brown I. Gereben M. Flicker
100	
101	

Distribution List for ARL-TR-88-17 under Contract N00014-87-K-0346
(cont'd)

Copy No.

102	School of Mechanical Engineering Georgia Institute of Technology Atlanta, GA 30332 Attn: P. Rogers
103	Department of Geology and Geophysics Geophysical and Polar Research Center Lewis G. Weeks Hall for Geological Sciences The University of Wisconsin, Madison 1215 W. Dayton Street Madison, WI 53706 Attn: C. S. Clay
104	Bolt, Beranek, & Newman, Inc. 1300 North 17th Street Arlington, VA 22209 Attn: R. Henrick H. Cox
105	Hawaii Institute of Geophysics The University of Hawaii 2525 Correa Road Honolulu, HI 96822 Attn: L. N. Frazer
106	F. K. Duennubier
107	Director North Atlantic Treaty Organization SACLANT ASW Research Centre APO New York 09019 Attn: T. Muir
108	F. Jensen
109	T. Akal
110	Library

Distribution List for ARL-TR-88-17 under Contract N00014-87-K-0346
(cont'd)

Copy No.

	Defence Research Establishment Pacific FMO Victoria, BC VOS 1B0 CANADA
111	Attn: N. R. Chapman
112	Library
	Defence Research Establishment Atlantic 9 Grove Street P.O. Box 1012 Dartmouth, NS CANADA
113	Attn: D. Chapman
114	Library
	Rosenteil School of Marine and Atmospheric Science Division of Ocean Engineering University of Miami Miami, FL 33149-1098
115	Attn: H. DeFarrari
116	T. Yamamoto
	Applied Physics Laboratory The Johns Hopkins University John Hopkins Road Laurel, MD 20810
117	Attn: J. Lombardo
118	G. Gillette
119	A. Boyles
120	R. Rottier
121	Library
	Department of Ocean Engineering Massachusetts Institute of Technology Cambridge, MA 02139
122	Attn: I. Dyer
123	A. Baggeroer
124	H. Schmidt

Distribution List for ARL-TR-88-17 under Contract N00014-87-K-0346
(cont'd)

Copy No.

125 The Catholic University of America
126 Washington, D. C. 20064
Attn: H. Uberall
J. J. McCoy

127 The University of Miami
10 Rickenbacker Causeway
Miami, FL 33149
Attn: F. Tappert

128 Department of Electrical Engineering
Polytechnic Institute of New York
Farmingdale, NY 11735
Attn: L. B. Felsen

129 I. Tolstoy
Knockvennie, Castle Douglas
S.W. SCOTLAND
GREAT BRITAIN

130 Department of Aerospace Engineering
131 and Engineering Mechanics
The University of Texas at Austin
Austin, TX 78712
Attn: A. Bedford
C. Yew

132 Department of Geology
The University of Texas at Austin
Austin, TX 78712
Attn: C. Wilson

133 Department of Physics
134 The University of Auckland
135 Private Bag, Auckland
NEW ZEALAND
Attn: A. C. Kibblewhite
C. T. Tindle
G. Bold

Distribution List for ARL-TR-88-17 under Contract N00014-87-K-0346
(cont'd)

Copy No.

	Defence Scientific Establishment HMNZ Dockyard Devonport, Auckland NEW ZEALAND
136	Attn: K. M. Guthrie
137	R. Bannister
138	Library
	Chinhae Research Laboratory P.O. Box 18 Chinhae, Kyeong Nam KOREA
139	Attn: Jungyul Na
	The Lamont-Doherty Geological Observatory Columbia University Palisades, NY 10964
140	Attn: R. D. Stoll
141	G. M. Bryan
	Department of Oceanography Texas A&M University College Station, TX 77843
142	Attn: A. Anderson
	Department of Physics The University of Texas at Austin Austin, Texas 78712
143	Attn: W. McCormick
144	A. W. Nolle
	Department of Mechanical Engineering The University of Texas at Austin Austin, Texas 78712
145	Attn: M. F. Hamilton
146	Nancy R. Bedford, ARL:UT
147	David T. Blackstock, ARL:UT
148	Eugene Brown, ARL:UT
149	Ilene J. Busch-Vishniac, ARL:UT

Distribution List for ARL-TR-88-17 under Contract N00014-87-K-0346
(cont'd)

Copy No.

150	Frederick Cotaras, ARL:UT
151	Glen E. Ellis, ARL:UT
152	Karl C. Focke, ARL:UT
153	Marshall E. Frazer, ARL:UT
154	David E. Grant, ARL:UT
155	Thomas A. Griffy, ARL:UT
156	Melanie Hafele, ARL:UT
157	James Hawkins, ARL:UT
158	John M. Huckabay, ARL:UT
159	Robert A. Koch, ARL:UT
160	Stephen Lind, ARL:UT
161	Stephen K. Mitchell, ARL:UT
162	Christopher Morfey, ARL:UT
163	David W. Oakley, ARL:UT
164	Susan G. Payne, ARL:UT
165	Clark S. Penrod, ARL:UT
166	F. Michael Pestorius, ARL:UT
167	Carol V. Sheppard, ARL:UT
168	Jack A. Shooter, ARL:UT
169	James Tencate, ARL:UT
170	Jacqueline N. Tjøtta, ARL:UT
171	Sigve Tjøtta, ARL:UT

Distribution List for ARL-TR-88-17 under Contract N00014-87-K-0346
(cont'd)

Copy No.

172	Bernard F. Tupa, ARL:UT
173	Evan K. Westwood, ARL:UT
174	Library, ARL:UT
175 - 189	Reserve, ARL:UT